Air-sea interactions in operational oceanography

Kai H. Christensen[1,2], Øyvind Breivik[1,3], and Graig Sutherland[4]

[1]Norwegian Meteorological Institute, Oslo, Norway
[2]University of Oslo, Oslo, Norway
[3]University of Bergen, Bergen, Norway
[4]Environment and Climate Change Canada, Montreal, Canada

May 28, 2021

Contents

1 Basic concepts **5**
- 1.1 Introduction 6
- 1.2 Dimensional analysis 9

2 Surface waves **15**
- 2.1 Solution for a single wave component in deep water 16
- 2.2 Mass, momentum and energy transport in surface gravity waves . 18

3 Spectral representation of surface waves **25**
- 3.1 Statistical properties of the surface wave field 26
- 3.2 The variance density spectrum 33
- 3.3 Wave energy balance equation 35
- 3.4 Wave action 36

4 Air-sea fluxes **39**
- 4.1 Air-sea fluxes 40
- 4.2 Wave-induced momentum and energy fluxes 47

5 Upper ocean turbulence **51**
- 5.1 The role of stratification 52
- 5.2 Diagnostic turbulence schemes 54
- 5.3 Prognostic turbulence schemes 59

6 Upper ocean drift currents **63**
- 6.1 Wind driven currents 64
- 6.2 Damped slab models of the upper ocean 67
- 6.3 The diurnal cycle in the upper ocean 68

6.4 Inertial oscillations with waves 72
6.5 Oceanic drift of buoyant materials 75

A Governing equations **77**
A.1 The material derivative 77
A.2 The mass conservation equation 77
A.3 The momentum equation 78
A.4 The Coriolis effect 78
A.5 Boussinesq approximation 79
A.6 The turbulence kinetic energy equation 79

Chapter 1

Basic concepts

1.1 Introduction

These lecture notes provide a brief introduction to the complex topic of upper ocean dynamics and air-sea interactions. Moreover, we put the emphasis on theories and methods that are of particular relevance in operational oceanography. There is a need for ocean forecasts much in the same way as there is a need for weather forecasts. A main difference is that the users of ocean forecasts are typically professional, requiring decision support for offshore operations, search-and-rescue missions, safe navigation, and so on, while weather forecasts are also relevant to the general public. What ocean and weather forecasting have in common is the focus on *transient features*, that is, how the states of the ocean and atmosphere change on short timescales, ranging from hours to perhaps a few weeks. Operational ocean modeling thus differs from ocean modeling in the context of climate research, in which the focus is often on the overall trends and not on day-to-day variations.

One of the most important uses of ocean forecast models is to provide predictions of drift trajectories, for example in the case of accidental oil spills or for ships that have lost their engine power. We are, therefore, not only concerned with the air-sea fluxes and the ocean circulation, but also on the behaviour of submersed or floating objects, large or small. This behaviour typically depends on the surface waves, the wind, the ocean currents, and quite often the turbulent mixing in the upper ocean; hence, such predictions require a complex collection of modelling tools. The purpose of these lectures is to provide an overview of such modelling tools and not an in-depth description of them, and the lectures will be complemented by project work in which some of these modelling tools are used to study specific physical mechanisms or applications.

Our focus is thus on the upper ocean. A good working definition of the "upper ocean" is given by Sprintall and Cronin (2001): "the upper ocean connects the surface forcing from winds, heat, and fresh water, with the quiescent deeper ocean where this heat and fresh water are sequestered and released on longer time and global scales", and they include both the surface mixed layer and the stratified layer below as part of the upper ocean. This definition highlights the different time rates of change of the processes in the upper and the deep ocean, respectively: upper ocean processes have temporal scales similar to that of the weather. We will primarily consider vertical exchange processes and vertical dynamical balances, that is, one-dimensional models of the upper ocean. The main reason for this restriction is that the processes responsible for rapid changes in the upper ocean

conditions are overwhelmingly acting in the vertical direction, and these processes can often be efficiently described with the simpler one-dimensional models. On the other hand, three-dimensional processes *are* tremendously important, both on large and small temporal and spatial scales (see Fig. 1.1), and we will repeatedly return to the question of how valid our one-dimensional models are. Furthermore, we will focus on open ocean conditions here and will not consider sea-ice dynamics or nearshore dynamics. Both of these topics are of course highly relevant in operational oceanography and merit dedicated study on their own.

We assume that the students know introductory geophysical fluid dynamics. The fundamental governing equations are, therefore, not derived in the running text, but instead listed in the Appendix for reference. Finally, a few words on notation. We will assume that the oceanic flow can be defined as a sum of (i) a mean flow, (ii) oscillatory motion due to surface waves, and (iii) turbulent motion. We, therefore, write the Eulerian velocity $\boldsymbol{u}$ as

$$\boldsymbol{u} = \bar{\boldsymbol{u}} + \tilde{\boldsymbol{u}} + \boldsymbol{u}', \tag{1.1.1}$$

where the overbar denotes mean quantities, the tilde denotes wave quantities, and the prime denotes turbulent quantities. We thus assume that the temporal scales T and spatial scales L are well separated, with $\bar{T} \gg \tilde{T} \gg T'$ and $\bar{L} \gg \tilde{L} \gg L'$. We also assume that this separation allows us to define averaging operators for removing turbulence and wave quantities. That is,

$$\{A\} = \{\bar{A} + \tilde{A} + A'\} = \{\bar{A}\} + \{\tilde{A}\} + \{A'\} = \bar{A}, \tag{1.1.2}$$

$$\langle A\rangle = \langle\bar{A} + \tilde{A} + A'\rangle = \langle\bar{A}\rangle + \langle\tilde{A}\rangle + \langle A'\rangle = \bar{A} + \tilde{A}, \tag{1.1.3}$$

for some quantity A. The averages can be in time, space or over a wave cycle, and the exact definitions will vary depending on the application. This scale separation is obviously convenient for the purpose of theoretical analysis, but some caution should be demonstrated. The kinetic energy spectrum of the ocean is continuous with no gaps, and a clear distinction between e.g. "wave motion" and "turbulent motion" can be hard to find. Also, processes that lead to upper ocean mixing can have a wide range of scales. For example, Langmuir circulation cells are large and slow compared to the surface waves that generate them, but their overall effect is to efficiently mix the upper ocean. From the point of view that the Langmuir cells are part of the "background turbulence[1]", we have in fact $\bar{T} \gg T' \gg \tilde{T}$ and $\bar{L} \gg L' \gg \tilde{L}$.

[1] Langmuir circulation is often referred to as Langmuir *turbulence*.

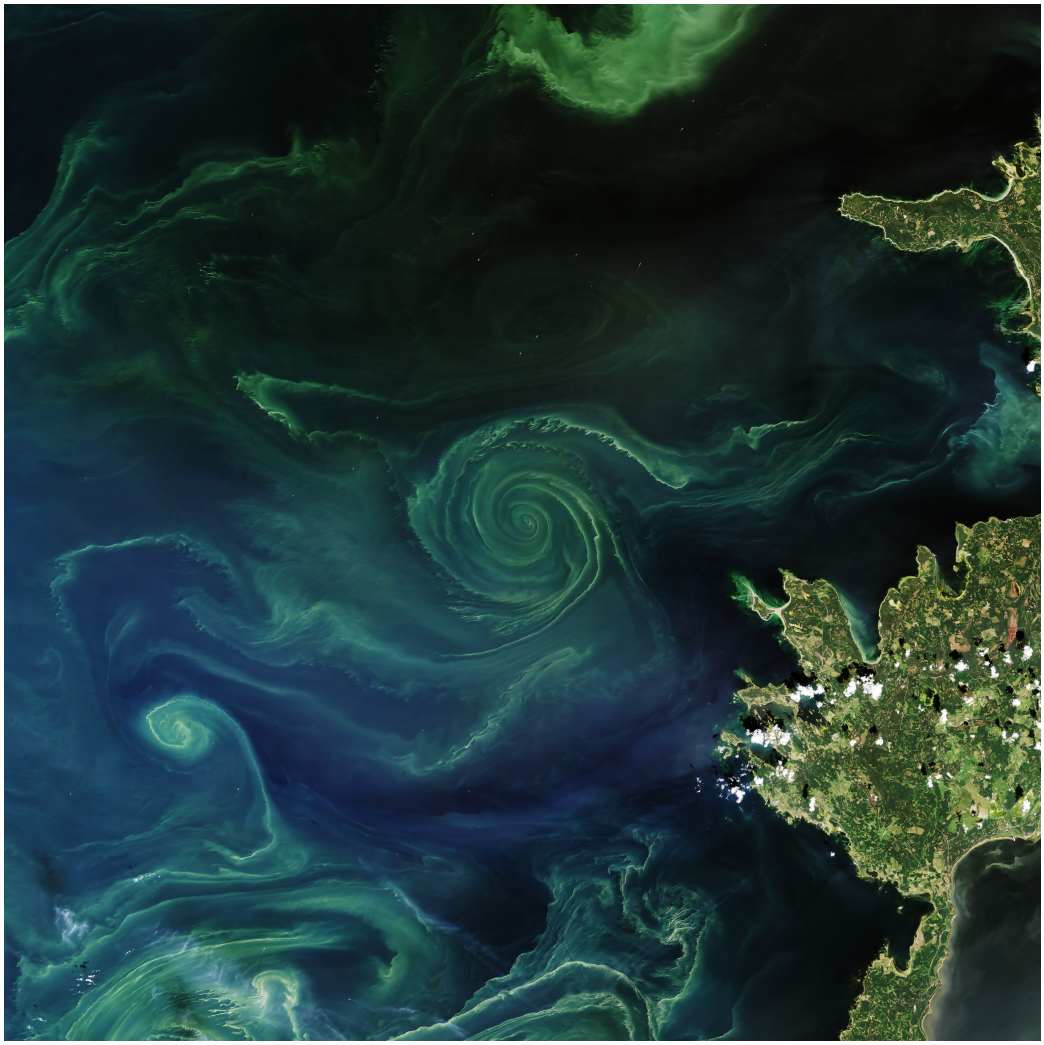

Figure 1.1: Blooms of cyanobacteria in the Gulf of Finland. The eddy in the middle is about 20-25 km across, and the image displays features over an impressive range of spatial scales, demonstrating the complex three-dimensional nature of geophysical fluid flows. Cyanobacteria (also called blue-green algae) can fixate nitrogen directly from the atmosphere and thrive in the nutrient-rich waters of the Baltic Sea. Image taken on July 18, 2018 from OLI/Landsat8 (NASA, Earth Observatory).

1.2 Dimensional analysis

1.2.1 The Pi Theorem

Dimensional analysis is a powerful tool to investigate the functional dependencies between different physical variables. The concept is based on the fact that any physical law needs to be unit free, that is, it should not matter what units are used to measure the fundamental physical dimensions such as time, distance, mass, and so on. The formal method we present here is due to Buckingham (1914) and is based on what is usually referred to as the (Buckingham) Pi Theorem:

Theorem. *Consider a physical law that includes m physical quantities $q_1, q_2, \ldots, q_m$. The corresponding n fundamental dimensions are given by $L_1, L_2, \ldots, L_n$. We require that $n < m$. The dimensions of q_i can be expressed in terms of the fundamental dimensions such that*

$$[q_i] = L_1^{a_{i1}} L_2^{a_{i2}} \cdots L_n^{a_{in}}, \quad i = 1, 2, \ldots, n. \tag{1.2.1}$$

We construct the $n \times m$ dimension matrix A from the exponents a_{ij}:

$$A = \begin{bmatrix} a_{11} & a_{12} & \cdots & a_{1m} \\ a_{21} & a_{22} & \cdots & a_{2m} \\ \vdots & \vdots & \ddots & \vdots \\ a_{m1} & a_{m2} & \cdots & a_{nm} \end{bmatrix}.$$

Let $r = \operatorname{rank}(A)$. If

$$f(q_1, q_2, \ldots, q_m) = 0 \tag{1.2.2}$$

is a unit free law, then we can form $m-r$ non-dimensional quantities $\pi_1, \ldots, \pi_{m-r}$, and (1.2.2) is equivalent to the equation

$$F(\pi_1, \pi_2, \pi_{m-r}) = 0, \tag{1.2.3}$$

which is expressed solely in the nondimensional quantities.

Later on in Section 2 we will discuss surface waves in more detail, but it is instructive to consider the example of wave dispersion here, that is, the relation between the wavelength and the wave period. The wave period is $T = 2\pi/\omega$ and the wavelength is $L = 2\pi/k$, where ω and k are the wave frequency and wave

number, respectively. We assume that there exists a function combining ω, k, the acceleration of gravity g and the water depth H. The fundamental quantities are

$$L_1 = \text{length}, \tag{1.2.4}$$
$$L_2 = \text{time}. \tag{1.2.5}$$

The coefficients of the dimension matrix are

$$[\omega] = L_2^{-1}, \quad \rightarrow \quad a_{11} = 0, a_{21} = -1, \tag{1.2.6}$$
$$[k] = L_1^{-1}, \quad \rightarrow \quad a_{12} = -1, a_{22} = 0, \tag{1.2.7}$$
$$[g] = L_1^1 L_2^{-2}, \quad \rightarrow \quad a_{13} = 1, a_{32} = -2, \tag{1.2.8}$$
$$[H] = L_2, \quad \rightarrow \quad a_{14} = 0, a_{24} = 1. \tag{1.2.9}$$

Hence we have

$$A = \begin{bmatrix} 0 & -1 & 1 & 1 \\ -1 & 0 & -2 & 0 \end{bmatrix}. \tag{1.2.10}$$

The matrix equation $A\boldsymbol{x} = 0$ has two independent solutions $\boldsymbol{x}_1 = [-2, 1, 1, 0]$ and $\boldsymbol{x}_2 = [0, 1, 0, 1]$. The dimensional variables are, therefore, given by (note that the order of the variables is important)

$$\pi_1 = \omega^{-2} k^1 g^1 H^0 = gk/\omega^2, \tag{1.2.11}$$
$$\pi_2 = \omega^0 k^1 g^0 H^1 = gH. \tag{1.2.12}$$

The physical law combining our physical parameters ω, k, g and H can then be expressed as

$$G(\pi_1, \pi_2) = 0. \tag{1.2.13}$$

We may solve this equation for one of the nondimensional variables, for example π_1, such that

$$\pi_1 = F(\pi_2) \rightarrow \frac{gk}{\omega^2} = F(kH) \tag{1.2.14}$$

for some unknown function F that can be determined from experiments. The solution (1.2.14) can be compared to the dispersion relation that we obtain by solving the dynamical equations:

$$\frac{gk}{\omega^2} = \frac{1}{\tanh(kH)}. \tag{1.2.15}$$

1.2.2 The Kolmogorov Spectrum

Another relevant example of dimensional analysis is that of Andrey Kolmogorov, who in the nineteen-forties did pioneering work on turbulence. He deduced the shape of the turbulence kinetic energy spectrum in the so-called inertial subrange. In this subrange, the turbulence kinetic energy (TKE) is assumed to be isotropic. The spatial scales are assumed less than the size of the dominant, energy containing eddies, and larger than the size of the smallest eddies that are dissipated into heat by viscosity. In the inertial subrange, the energy is said to cascade from larger to smaller scales. The TKE input is obviously on the larger scales while the TKE loss is at the smallest scales in the range, see Fig. 1.2.

The smallest temporal and spatial scales are the so-called Kolmogorov microscales. At these scales the relevant physical quantities are the (kinematic) viscosity, ν, and the TKE dissipation rate, ϵ. The dimension of the dissipation rate is length^2/time^3, while the viscosity has dimension length^2/time. The only length scale we can derive from these quantities is

$$l_K = \left(\frac{\nu^3}{\epsilon}\right)^{\frac{1}{4}}, \tag{1.2.16}$$

which is known as the Kolmogorov length. Similarly, we can derive a Kolmogorov time scale $t_K = \sqrt{\nu/\epsilon}$.

In the inertial subrange we disregard viscous dissipation, however, and the fundamental quantities are the turbulent velocity fluctuations, v, say, and the size of the turbulent eddies, l. These quantities can be combined into a time scale $T = l/v$. We introduce the wavenumber $\kappa = l^{-1}$ and the energy spectrum $E(\kappa)$ (strictly speaking, E is the velocity variance spectrum) such that the energy $\mathcal{E}$ contained in eddies in the wavenumber range κ to $\kappa + \mathrm{d}\kappa$ is given by

$$\mathcal{E} = E(\kappa)\mathrm{d}\kappa. \tag{1.2.17}$$

The TKE is by definition proportional to the square of the velocity fluctuations, that is

$$\mathcal{E} \propto v^2. \tag{1.2.18}$$

Now we assume that the rate at which energy is lost is constant across the inertial subrange, which means that

$$\frac{\mathcal{E}}{T} = \frac{v^2}{(l/v)} = \text{const.} \tag{1.2.19}$$

It follows that the turbulent velocity fluctuations and the turbulence length scales have to be related in such a way that $v \propto l^{1/3} = \kappa^{-1/3}$. Using this result, together with (1.2.17) and (1.2.18), we find that the TKE scales as

$$E(\kappa)\mathrm{d}\kappa \propto \kappa^{-\frac{2}{3}}, \tag{1.2.20}$$

which means that the TKE *spectrum* scales as

$$E(\kappa) \propto \kappa^{-\frac{5}{3}}. \tag{1.2.21}$$

Kolmogorov's derivation includes the dissipation rate as well (the original paper is in Russian, so this is second-hand information, but a compact derivation along with instructive real-life examples can be found in Ortiz-Suslow et al., 2020). Assuming a functional relationship between E, ϵ and κ, straightforward application of the Pi Theorem shows that

$$E(\kappa) = \alpha\epsilon^{\frac{2}{3}}\kappa^{-\frac{5}{3}}, \tag{1.2.22}$$

where α is a constant.

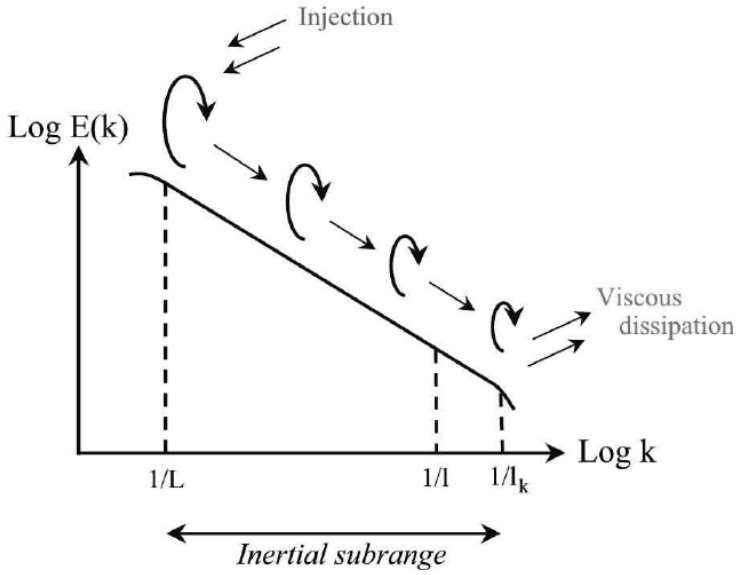

Figure 1.2: Schematic representation of the energy cascade and the inertial subrange. The mean flow provides the energy input on the longest scales, while energy is dissipated at the smallest scales, which are given by the Kolmogorov length. In the inertial subrange the turbulence kinetic energy spectrum decays as $\kappa^{-5/3}$ *(credit: "Aakash30jan"/Wikimedia Commons).*

Chapter 2

Surface waves

This chapter contains a short recap of central concepts in surface wave dynamics. The main aim of this chapter is to introduce the *Stokes drift*, which is the mean momentum in surface waves and a key component of the drift velocity in the upper ocean.

2.1 Solution for a single wave component in deep water

A plane wave can generally be described as a function

$$\boldsymbol{v} = \boldsymbol{f}(\theta),$$

where $\theta = \boldsymbol{k} \cdot \boldsymbol{x} - \omega t + \delta$ is a phase function. Here $\boldsymbol{k} = (k, l)$ is the wave number vector, ω is the circular wave frequency (radians per second) and δ is a constant phase shift (radians). The associated wave period and wavelength are $T = 2\pi/\omega$ and $\lambda = 2\pi/\kappa$, respectively, where $\kappa = \sqrt{k^2 + l^2}$. The wave number vector defines the direction of wave propagation, and the ratio between the wave frequency and wave number, that is $c \equiv \omega/\kappa$ defines the propagation speed, or *phase speed* of the wave. The direction of wave propagation is $\boldsymbol{i}_\kappa = (k, l)/\kappa$ such that we can define the phase velocity as $\boldsymbol{c} = c\,\boldsymbol{i}_\kappa$.

The equations that describe surface wave motion can be derived in different ways. We will here follow Gill (1982) and focus on the pressure perturbation in the waves. We define this pressure perturbation as $\tilde{p}$, and take the pressure to be $p = p_0 - \rho g z + \tilde{p}$. Assuming the fluid is incompressible, from the continuity equation we have

$$\boldsymbol{\nabla} \cdot \boldsymbol{v} = 0, \tag{2.1.1}$$

and from the linearized equations, ignoring friction and the Coriolis force (we assume that rotational effects are negligible for the wave motion since the wave periods are so small, but, as we shall see later on, this is not quite correct for the wave-induced drift) we have

$$\rho \frac{\partial \boldsymbol{v}}{\partial t} = -\boldsymbol{\nabla} \tilde{p}. \tag{2.1.2}$$

Taking the time derivative of (2.1.1) and combining it with (2.1.2), we find that the perturbation pressure is governed by

$$\nabla^2 \tilde{p} = 0, \tag{2.1.3}$$

hence $\tilde{p}$ is a harmonic function.

We are primarily interested in surface gravity waves in deep water and take the water depth to be infinite. In practice we only need to require that the ratio between the wavelength λ and the local water depth H is such that $\lambda/H \ll 1$, but the above assumption simplifies the analysis. Thus, as $z \to -\infty$, we require that the pressure perturbation and the velocities vanish. At the surface $z = \eta$, we have one kinematic boundary condition and one dynamic boundary condition. The kinematic boundary condition simply expresses that the vertical velocity at the surface is the same as the vertical velocity of the surface itself. To leading order this becomes

$$w = \frac{\partial \eta}{\partial t}, \qquad z = 0. \tag{2.1.4}$$

The dynamic boundary condition expresses that the pressure at the surface is equal to the atmospheric pressure p_0. Since we have $p(z = \eta) = p_0 - \rho g \eta + \tilde{p}$, we have

$$\tilde{p} = \rho g \eta, \qquad z = \eta. \tag{2.1.5}$$

The perturbation pressure $\tilde{p}$ in a single wave component can be found postulating a solution

$$\tilde{p} = G(z) \cos(kx + ly - \omega t + \delta). \tag{2.1.6}$$

Inserting (2.1.6) into (2.1.3), and using the requirement that $\tilde{p} \to 0$ as $z \to -\infty$, we obtain

$$\tilde{p} = A e^{\kappa z} \cos(kx + ly - \omega t + \delta), \tag{2.1.7}$$

where $\kappa = \sqrt{k^2 + l^2}$ is the wave number and A is a constant[1]. We now assume that the surface elevation is given by

$$\eta = a \cos(kx + ly - \omega t + \delta), \tag{2.1.8}$$

that is, in phase with the pressure perturbation. Here a is the amplitude of the wave component. Combining (2.1.2), (2.1.4) and (2.1.8), we find for the integration constant A:

$$A = \rho \frac{a\omega^2}{\kappa}. \tag{2.1.9}$$

[1]More general solutions can be found assuming $G = G(z, t)$, in which case A can be a function of time. It is also possible to allow G to be a function of *all* the spatial coordinates, assuming small amplitude changes over the length and time scales given by the wavelength and wave period.

The ratio between the wave height and the wavelength is expressed by the wave steepness, $\varepsilon \equiv a\kappa$. The propagation speed, or *phase speed*, of the waves is given by $c = \omega/\kappa$. Hence we can write the pressure perturbation in the waves as

$$\tilde{p} = \rho\varepsilon c^2 \mathrm{e}^{\kappa z} \cos(kx + ly - \omega t + \delta). \tag{2.1.10}$$

We note that the pressure is linear in the wave steepness, quadratic in the phase speed, and that it vanishes at a depth of $O(\kappa^{-1})$, which is proportional to the wavelength λ. The *Stokes depth* $(2\kappa)^{-1}$ is often used as a typical depth scale for the influence of the waves. Recall, however, that we are here only considering gravity waves in deep water. In shallow water ($\lambda \geq H$) the wave motion extends throughout the water column (e.g. Gill, 1982).

The next thing we need to do is to find the relation between ω and κ. We linearize (2.1.10), noting that $\tilde{p}(z = \eta) = \tilde{p}(z = 0) + O(a^2)$. Combining with the dynamic boundary condition (2.1.5), we obtain

$$\omega^2 = g\kappa. \tag{2.1.11}$$

This is the *dispersion relation* that enables us to relate the wave frequency to the wavelength. Note that (2.1.11) is a special case of the relation (1.2.14) that we derived using dimensional analysis. For the phase speed we have

$$c = \pm\sqrt{\frac{g}{\kappa}} = \pm\sqrt{\frac{g\lambda}{2\pi}}. \tag{2.1.12}$$

2.2 Mass, momentum and energy transport in surface gravity waves

The energy in a wave component is the sum of the potential and kinetic energy. The velocities can be obtained from the linearized momentum equation (2.1.2), and the kinetic energy is

$$E_\mathrm{k} = \int_{-\infty}^{\eta} \frac{\rho}{2}\{\tilde{\boldsymbol{u}}^2\}\,\mathrm{d}z = \frac{1}{4}\rho g a^2, \tag{2.2.1}$$

where we have used the dispersion relation (2.1.11). Setting the reference level at the undisturbed surface $z = 0$, the potential energy is given by

$$E_\mathrm{p} = \int_{0}^{\eta} \rho g z\,\mathrm{d}z = \frac{1}{4}\rho g a^2. \tag{2.2.2}$$

We see that the kinetic and potential energies are equal. This is a general property of surface waves and is usually referred to as the "equipartition principle". The total energy in the waves becomes $E_{\mathrm{tot}} = E_{\mathrm{k}} + E_{\mathrm{p}} = (\rho g a^2)/2$.

The transport of energy in the waves is a curious concept. We have already established that a single wave component propagates with a speed c, but in reality the sea state is the sum of many wave components with different phases, amplitudes, periods, wavelengths and directions, which leads to some interesting results. The classical way of introducing the energy transport in surface waves is to add two components of nearly equal wave frequencies and wave numbers. Consider two such wave components propagating in the positive x-direction. From standard trigonometric identities we can write this sum as

$$a\cos[(k-\Delta k)x-(\omega-\Delta\omega)t)+a\cos[(k+\Delta k)x-(\omega+\Delta\omega)t)= 2a\cos(kx-\omega t)\cos(\Delta kx-\Delta\omega t). \tag{2.2.3}$$

The result is a wave of twice the amplitude $2a\cos(kx-\omega t)$ that is modulated by the function $\cos(\Delta kx-\Delta\omega t)$. This function is in itself just like a single wave component, but with a speed given by $\Delta\omega/\Delta k$. Since Δk and $\Delta\omega$ are assumed small, this wave component is much longer than both of the original components, and with much longer period. Hence we can view the sum of the two nearly equal wave components as one wave component with twice the amplitude and the average wave number and wave frequency, which is enveloped by a much longer wave. The energy in the waves are contained within this envelope, or wave group, and hence advected with the propagation speed $\Delta\omega/\Delta k$. We now use the limits $\Delta k\to 0$ and $\Delta\omega\to 0$ and define the group velocity

$$c_{\mathrm{g}} = \frac{\partial\omega}{\partial\kappa}. \tag{2.2.4}$$

For deep water waves it is easy to show from (2.1.11) that $c_{\mathrm{g}} = c/2$. As the waves propagate into shallower water, the ratio c_{g}/c increases until we have $c_{\mathrm{g}} = c$ in the limit $kH\to 0$ when the wavelength is much larger than the local depth.

Static figures like 2.1 can illustrate the "groupiness" of surface waves, but cannot really be used to illustrate the difference between the phase and group *velocities*. There are some excellent animations on the Internet, however, see for example the Wikipedia entry for the group velocity[2].

[2] https://en.wikipedia.org/wiki/Group_velocity

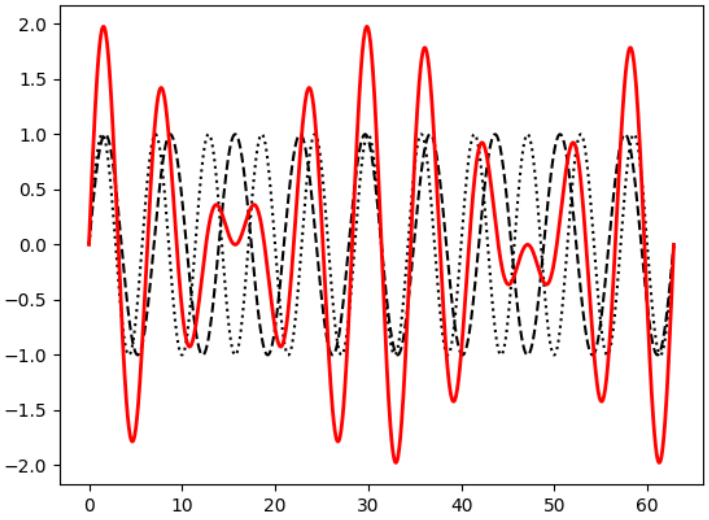

Figure 2.1: The functions $sin(1.1x)$ (dotted), $sin(0.9x)$ (dashed), and their sum (solid).

The trajectories of fluid parcels due to the waves can, as a first approximation, be obtained by integrating the velocities in time:

$$\tilde{\boldsymbol{x}} = (\tilde{x}, \tilde{y}, \tilde{z}) = \left(\int \tilde{u}\, \mathrm{d}t, \int \tilde{v}\, \mathrm{d}t, \int \tilde{v}\, \mathrm{d}t \right). \tag{2.2.5}$$

Inserting for the wave velocities the fluid parcels describe closed trajectories. For deep water waves propagating in the positive x-direction:

$$(\tilde{x}, \tilde{z}) = a\mathrm{e}^{-kz} \left(\cos(kx - \omega t), \sin(kx - \omega t) \right), \tag{2.2.6}$$

indicating that the deep water wave trajectories are perfect circles with radii that decay exponentially with depth. We will see below that this is only correct to first order in the wave steepness.

It appears from (2.2.6) that there is no net transport of mass in the waves. Any fluid parcel will return to its initial position after a wave period. We do know, however, that surface waves (and many other types of waves) are associated with a mean drift velocity. Consider any point in the fluid that is *above* the wave troughs, that

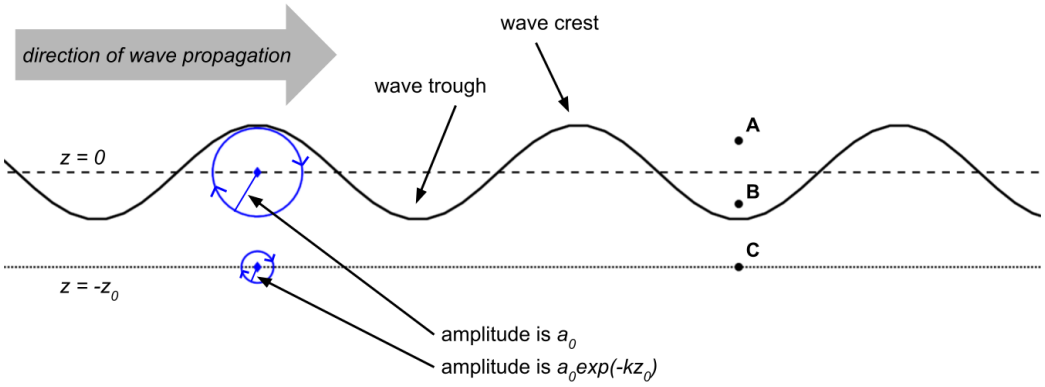

Figure 2.2: In a linear description of the wave motion the particles travel in closed orbits. Here this is illustrated by the two circles at depths $z = 0$ and $z = -z_0$, implying that these are deep water waves (the orbits become increasingly elliptic towards shallow water). Any particle under the wave crest will have a velocity in the wave propagation direction, while the velocity is against the wave propagation direction under the wave troughs. Eulerian (fixed point) measurements of the velocity of the water in the three locations indicated on the right will show that at (A) there is air for most of the wave cycle, with intermittent flow of water in the wave propagation direction associated with passing crests; at (B) there is water for most of the wave cycle, with velocities in both horizontal directions, but on average in the wave propagation direction; while at (C) there is water during the whole wave cycle with an average velocity of zero.

is $z > -a$. Under the wave crest, we have zero vertical velocity and maximum horizontal velocity in the wave propagation direction. Under the wave trough, we also have zero vertical velocity and maximum velocity opposite to the wave propagation direction. Above the wave trough there is only air, however, which means that there is no transport of water. At any specific point above the wave troughs, the transport of water is, therefore, *on average* going in the wave propagation direction, while below the wave troughs the net mass transport is zero (see Fig. 2.2).

The description above is based on the Eulerian description of the fluid motion. It is more instructive, and also more relevant to oceanic transport problems, to consider the wave-induced drift from a Lagrangian perspective. In the Lagrangian description we label each fluid parcel and follow them in time, in contrast to the

Eulerian description in which we stay in fixed positions and note the velocities of the fluid parcels that happen to flow by. It is clear that we do not need to consider the somewhat awkward case "sometimes air, sometimes water" if we are using a Lagrangian description of the motion. We are, after all, following individual fluid parcels that maintain their material properties.

A direct Lagrangian approach has its merits, in particular when studying wave-induced drift (Weber, 2019), but we will not use it here. We will instead use a quasi-Lagrangian description introduced by Longuet-Higgins (1953). The point is to evaluate the Eulerian velocities at the positions traced by the fluid parcels. That is, we write the Lagrangian velocity as

$$\boldsymbol{u}_{\mathrm{L}} = \boldsymbol{u}(\boldsymbol{x} + \tilde{\boldsymbol{x}}, t). \tag{2.2.7}$$

The next thing we do is to make a first order Taylor expansion of the righthand-side, such that

$$\boldsymbol{u}(\boldsymbol{x} + \tilde{\boldsymbol{x}}, t) \approx \boldsymbol{u}(\boldsymbol{x}, t) + \tilde{\boldsymbol{x}} \cdot \boldsymbol{\nabla} \boldsymbol{u}. \tag{2.2.8}$$

Recall that the Eulerian velocity consists of mean, wave and turbulent parts so that $\boldsymbol{u} = \bar{\boldsymbol{u}} + \tilde{\boldsymbol{u}} + \boldsymbol{u}'$, and that curly brackets imply averaging over a wave cycle. When averaging, we get from (2.2.8)

$$\{\boldsymbol{u}(\boldsymbol{x}, t) + \tilde{\boldsymbol{x}} \cdot \boldsymbol{\nabla} \boldsymbol{u}\} = \bar{\boldsymbol{u}} + \{\tilde{\boldsymbol{x}} \cdot \boldsymbol{\nabla} \tilde{\boldsymbol{u}}\}. \tag{2.2.9}$$

The latter part is called the Stokes drift velocity (Stokes, 1847), which we will denote by $\bar{\boldsymbol{u}}_{\mathrm{S}}$. For deep water waves we have

$$\bar{\boldsymbol{u}}_{\mathrm{S}} = \{\tilde{\boldsymbol{x}} \cdot \boldsymbol{\nabla} \tilde{\boldsymbol{u}}\} = (\varepsilon^2 \boldsymbol{c}) \mathrm{e}^{-2\kappa z}. \tag{2.2.10}$$

The difference between the Eulerian and Lagrangian description of the Stokes drift is illustrated in Fig. 2.3. We define the Lagrangian *mean* velocity $\bar{\boldsymbol{u}}_{\mathrm{L}}$. Correct to second order in the wave steepness, we now have

$$\bar{\boldsymbol{u}}_{\mathrm{L}} = \bar{\boldsymbol{u}} + \bar{\boldsymbol{u}}_{\mathrm{S}}. \tag{2.2.11}$$

A couple of comments are in place here. First of all, the Lagrangian mean velocity is the drift velocity of any neutrally buoyant object that is in the water, and which is sufficiently small so that inertia can be neglected. This is the case for some types of nutrients, plankton and pollution, and approximately the case also for many types of buoyant small objects (e.g. pelagic fish eggs or oil droplets), although, as we will see later on, the vertical motion of such objects relative to

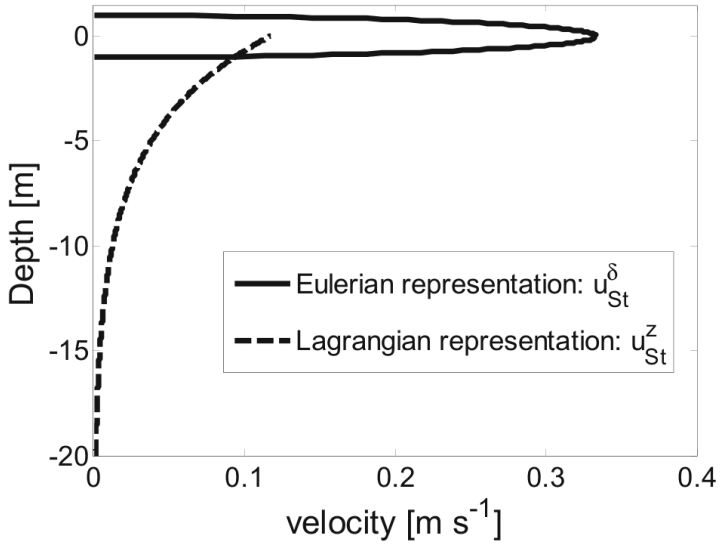

Figure 2.3: The mean drift velocity in deep water surface waves with amplitude of 1 m and a period of 6 s. In the Eulerian description, the transport is confined to the region between the wave trough and wave crest since the average wave velocities below this region are zero. In the Lagrangian description, however, the wave drift is represented by the Stokes drift, which for deep water waves decays exponentially away from the surface. The total transport, and hence the mean wave momentum, is the same in both the Lagrangian and Eulerian descriptions. From Broström et al. (2014).

the water is very important for determining the horizontal mean drift because of the high vertical shear close to the surface. Second, numerical ocean circulation models are overwhelmingly using an Eulerian framework, solving for $\bar{\boldsymbol{u}}$. Hence the Lagrangian mean velocity that is so important for oceanic drift modeling will need to be calculated using (2.2.11), which generally requires additional output from a numerical wave prediction model for calculating $\bar{\boldsymbol{u}}_{\mathrm{S}}$.

Finally, since there is a mean forward drift velocity in the waves, it follows that the waves possess mean momentum. The total mean momentum in the waves (per unit surface area) is given by

$$\boldsymbol{M}_{\mathrm{w}} = \rho \boldsymbol{U}_{\mathrm{S}} = \rho \int_{\infty}^{0} \bar{\boldsymbol{u}}_{\mathrm{S}} \, \mathrm{d}z. \tag{2.2.12}$$

The wave field thus acts as a reservoir of mean momentum, and spatial and tem-

poral changes in the wave field is associated with momentum fluxes between the waves and the atmosphere, and the waves and the mean oceanic flows, a subject that will be discussed in more detail in Sec. 4.

Chapter 3

Spectral representation of surface waves

In this chapter we focus on the spectral representation of the surface wave field and the energy balance equation. The source terms in this equation describe the growth and dissipation of the waves, as well as the transfer of energy between different wave components. The source terms are also used to quantify the wave-induced momentum and energy fluxes that influence the mean flows in the ocean.

3.1 Statistical properties of the surface wave field

By assuming that the wave field is stationary and homogeneous, that is, its statistical properties are unchanging in time and space—clearly an unrealistic assumption—and by furthermore assuming that the wave field decorrelates in a finite distance, we can formally employ the Fourier transform to define a power density spectrum of a time series of the surface elevation. Less formally, and hopefully more understandably, what this means is that we can identify those waves (sinusoids to a first approximation) that make up the wave field. In a one-dimensional sea (which literally never occurs), we can simplify this picture further to those waves that travel either to the left or to the right.

3.1.1 The variance of a monochromatic wave

Consider first a monochromatic wave whose elevation is $\eta = a\cos(kx - \omega t + \delta)$, similar to Eq (2.1.8), but in one spatial dimension, x, only. The mean square or variance (since η has zero mean) is found by taking the temporal average over one wave period $T = 2\pi/\omega$, that is, by integrating η^2 over one wave period T and dividing by T,

$$\{\eta^2\} = \frac{1}{T}\int_0^T a^2\cos^2\frac{2\pi t}{T}\,\mathrm{d}t. \tag{3.1.1}$$

Since we know [see e.g. Gradshteyn and Ryzhik 2007, Eq (2.513-11), p 154] that

$$\int_0^{2\pi}\cos^2 t\,\mathrm{d}t = \pi, \tag{3.1.2}$$

it follows after an elementary variable substitution of $u = 2\pi t/T$ which leads to $\mathrm{d}t = \frac{T\mathrm{d}u}{2\pi}$ (the integral now goes from $u_0 = 0$ to $u_1 = \frac{2\pi T}{T} = 2\pi$) that $\{\eta^2\} = a^2/2$. This demonstrates that the variance of the surface elevation is proportional to the square of the amplitude for a monochromatic wave (a single sine wave). It also shows that by multiplying the wave variance by ρg we get the total energy, E_{tot}, see Eqs (2.2.1)–(2.2.2).

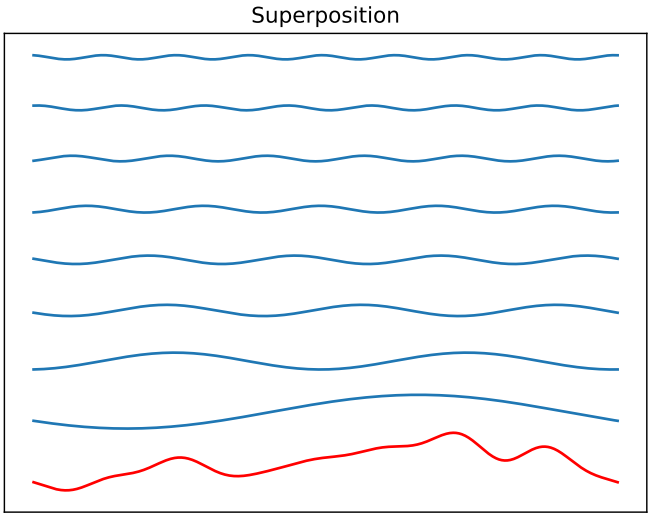

Figure 3.1: Eight sinusoids (blue) with different frequencies and phases δ_n superposed create a complex-looking time series (red).

3.1.2 Superposition of sinusoids—The Fourier series

Any discrete and evenly sampled time series $\eta(t_i)$ where the measurements are taken at times $t_n = (n-1)\Delta t, n = 1, 2, ..., N$ and the length of the domain is T can be represented *exactly* as a Fourier series of cosines,

$$\eta(t) = \frac{a_0}{2} + \sum_{n=1}^{N} a_n \cos\left(\tfrac{2\pi n t}{T} - \delta_n\right). \tag{3.1.3}$$

So a sum of (co)sines with different amplitudes, frequencies and phases can be fitted to a finite set of measurements. As shown conceptually in Fig 3.1, a surprisingly small number (eight here) of sine waves when superposed can create quite complex-looking time series.

3.1.3 The autocovariance function

Unfortunately, an infinite time series has infinite energy and cannot be represented as a Fourier series. To represent the *variance* of the different wave components

present on the sea surface, we look instead at the *autocovariance* of the surface. We ask "How do water level measurements correlate with other water level measurements separated by a length of time τ?". It seems natural that measurements that are close in time are also strongly correlated (if you measure the peak of a wave, you expect the next measurement a fraction of a second later to also be high, likewise, a measurement in a trough will be followed by another measurement low down). If we are not specifically interested in the *phase* of the sine waves, only their amplitudes, we can use the discrete autocovariance function

$$R_{\eta\eta}(\tau) = \sum_{n=1}^{N} \eta(t_n)\eta(t_n + \tau). \tag{3.1.4}$$

This function will presumably die off for large τ since we don't expect a wave hundreds of wave periods later (or hundreds of wavelengths down-wave in space) to be in phase with our measurement here and now. We say that waves *decorrelate* in time and space. This makes the autocovariance function approach zero for large time lags τ and its integral remain finite,

$$\int_{-\infty}^{\infty} |R_{\eta\eta}|^2 \, \mathrm{d}\tau < \infty. \tag{3.1.5}$$

In Fig 3.2 we see a time series of 20 minutes (and a zoom of the first 150 seconds in Fig 3.3) sampled twice a second with a nadir-looking radar altimeter at the Ekofisk field in the central North Sea. It is evident that the waves are irregular in shape, but also that they have a dominant period of about 10 seconds. How will measurements covary with other measurements taken at a later time? This is what Eq (3.1.4) answers, and Fig 3.4 shows what the autocovariance of Fig 3.3 out to time lags of 75 seconds is like. As expected, the autocovariance is strongest at a time lag of zero. This simply means that measurements covary perfectly with themselves, as of course they must! We can calculate the significant wave height directly from the time series in Fig 3.3,

$$H_\mathrm{s} = 4\sqrt{\frac{1}{N}\sum_{n=1}^{N} \eta(t_n)^2}. \tag{3.1.6}$$

This is sometimes referred to as $H_{4\mathrm{rms}}$ because it is four times the standard deviation (or root-mean-square of a zero-mean process). This shows that the significant wave height is "4σ", which is quite far from the "average" wave height. This is

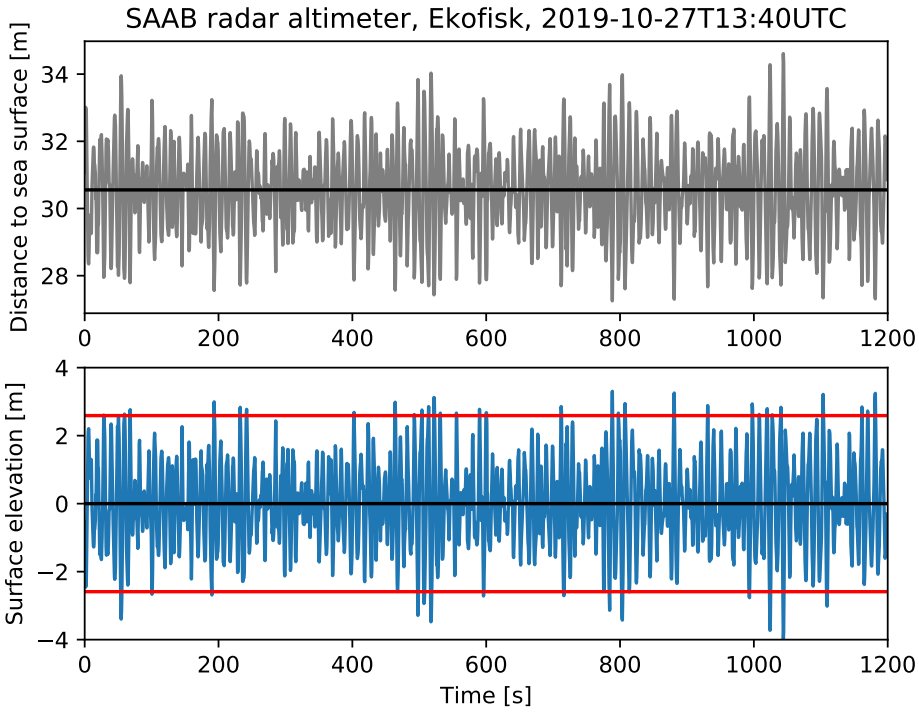

Figure 3.2: A 2 Hz 20-minute time series of the water elevation as measured by a SAAB radar altimeter from approximately 30.5 m height. In grey (upper panel) is shown the distance to the sea surface (what the radar altimeter measures), and in blue (lower panel) the elevation above a mean sea level (the inverse of the zero-mean time series). Also shown as two red lines is the significant wave height, H_s.

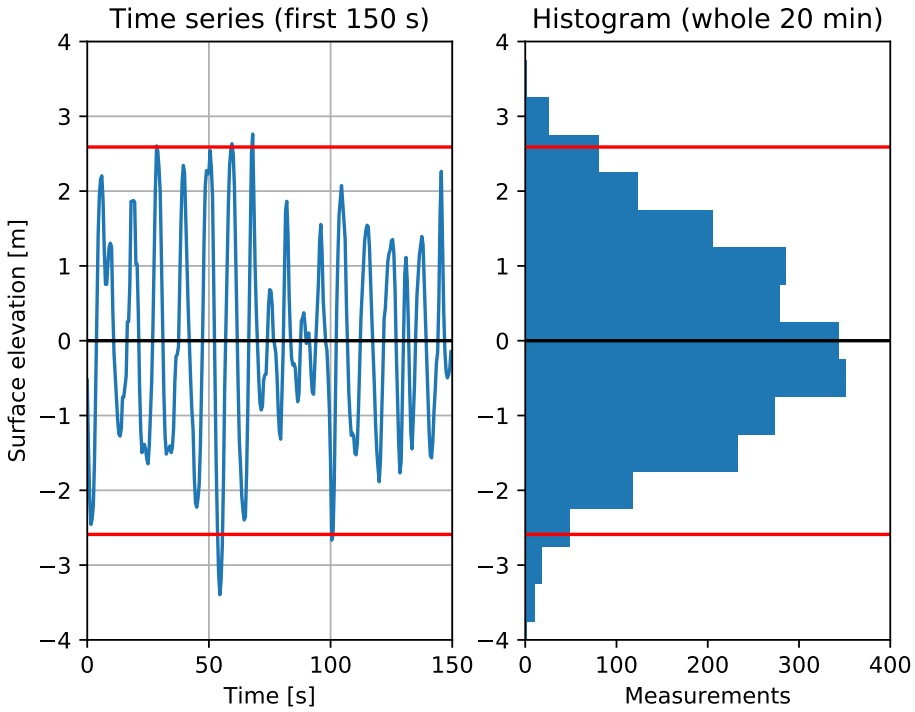

Figure 3.3: A closer look at the first 150 seconds (left) and a histogram of the water elevation measurements throughout the 20 minutes depicted in Fig 3.3. It is evident from the histogram that H_s envelops a very high portion (about 95%) of the measurements, as expected as $H_s = 4\sigma$, that is, the red lines are located as $\pm 2\sigma$, where σ is the standard deviation of the surface height η.

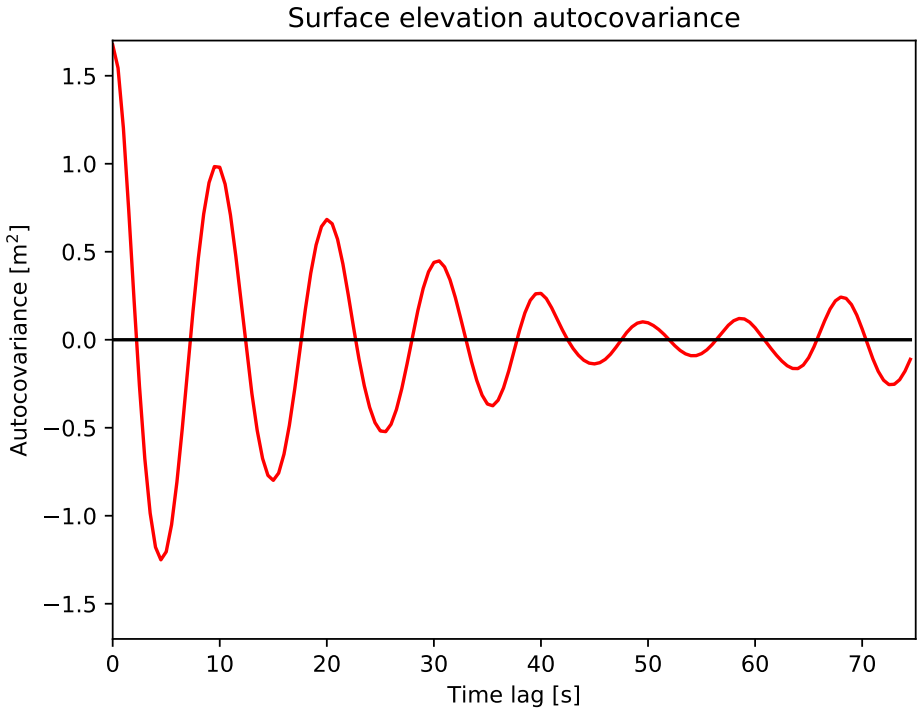

Figure 3.4: The autocovariance function of the time series in Fig 3.3.

easy to see in Fig 3.3 where the distance between the red lines is the significant wave height. In fact, we can read off the *variance* of the time series at time lag zero in Fig 3.4. Knowing that the significant wave height is four standard deviations of the water level, and seeing that the variance is approximately $1.67\,\mathrm{m}^2$, we find that $H_\mathrm{s} \approx 4\sqrt{1.67} \approx 5.2\,\mathrm{m}$ in this case.

More to the point for our discussion of waves of different periods is the observation that the first "trough" in our autocovariance function occurs at a time lag of about 5 seconds. This means that the strongest *negative* correlation between measurements is found at a separation of 5 seconds. This means that measurements separated by this time lag disagree the most, which is what we expect after *half* a wave period since a measurement at a wave crest is the opposite (high) of a wave trough. Moving on to the first peak of our autocovariance function we see that it occurs after a time lag of about 10 seconds. This is precisely what we would expect following our visual inspection of Fig 3.3. The measurements that are separated by about 10 seconds are mostly (but not perfectly—note the irregular shape of the waves in Fig 3.3) in phase.

Now imagine that we take the integral of the square of the autocovariance function in Fig 3.4. It seems to be trailing off for large time lags. In fact, it will approach zero, although not perfectly. However, if we accept that the remaining weak covariance at long time lags is just the product of random coincidence, we can assume that the true covariance of the wave field decays to zero. This means that we have a function which, like we anticipated in Eq (3.1.5), is *bounded*, that is, not infinite when integrated to infinite time lags. Such a function has a frequency-domain counterpart which can be found using the *Fourier transform*. Defining the frequency $f = \omega/2\pi$:

$$G(f) = \int_{-\infty}^{\infty} R\mathrm{e}^{-\mathrm{i}2\pi f\tau}\,\mathrm{d}\tau. \tag{3.1.7}$$

We have now dropped the subscripts on R for brevity. This integral is generally complex, but is real for even (symmetric) functions. Conveniently, the autocovariance $R(\tau)$ of a time series is even, which can most easily be understood by imagining that we correlate observations that are separated by a *negative* time lag. Clearly it shouldn't matter whether we compare the first $N-k$ measurements $1, 2, ..., N-k$ with the last $N-k$ measurements, $k+1, k+2, ..., N$ or vice versa. This proves that a negative time lag $\tau = -k\Delta t$ should give the same result as the positive time lag $k\Delta t$ and the autocovariance must be symmetric (even) function about zero time lag.

3.2 The variance density spectrum

The quantity $G(f)$ in Eq (3.1.7) is known as the *power spectral density*, or in our parlance, the *variance density spectrum*. We are now ready to calculate it from our time series in Fig 3.3.

First, the *discrete* Fourier transform of the time series is constructed,

$$\hat{\eta}(f_k) = \sqrt{\frac{\Delta t}{N}} \sum_{n=0}^{N-1} \eta(t_n) \exp\left(2\pi \mathrm{i} k n/N\right) \tag{3.2.1}$$

The Fourier coefficients are generally complex, and there are as many frequencies as there are points in the time series,but half of them are negative, $-f_k = f_{-k}, k = 0, 1, ..., N/2$. To get to the *power spectral density*, which is what is needed for the variance density spectrum, we must now find the squared modulus of the positive and negative frequencies, which is a real number,

$$F(f_k) = |\hat{\eta}(f_k)|^2 + |\hat{\eta}(-f_k)|^2. \tag{3.2.2}$$

This is called the *periodogram* method and the variance density spectrum of our time series in Fig 3.3 is shown in Fig 3.5. The variance density spectrum shows us how the variance is distributed over frequencies. To better understand what is meant by this, we return to the variance density of a monochromatic wave as in 3.1.1 By integrating the spectrum we get the total variance of the time series,

$$E = \int_0^\infty F(f)\,\mathrm{d}f. \tag{3.2.3}$$

This should then equal var(η). This is formally known as Parseval's theorem which here means that the total wave energy of the spectrum is the same as the average wave energy of the time series.

Let us now look at how the variance density is related to the variance of a single sine wave (3.1.1). If our spectrum consisted of this one frequency band, the variance density spectrum is simply

$$F_k = \frac{1}{2} a_k^2 / \Delta f_k, \tag{3.2.4}$$

and since there is only one frequency, $k = 1$. As we add more frequency bands, the superposition principle tells us that they can be added to each other without

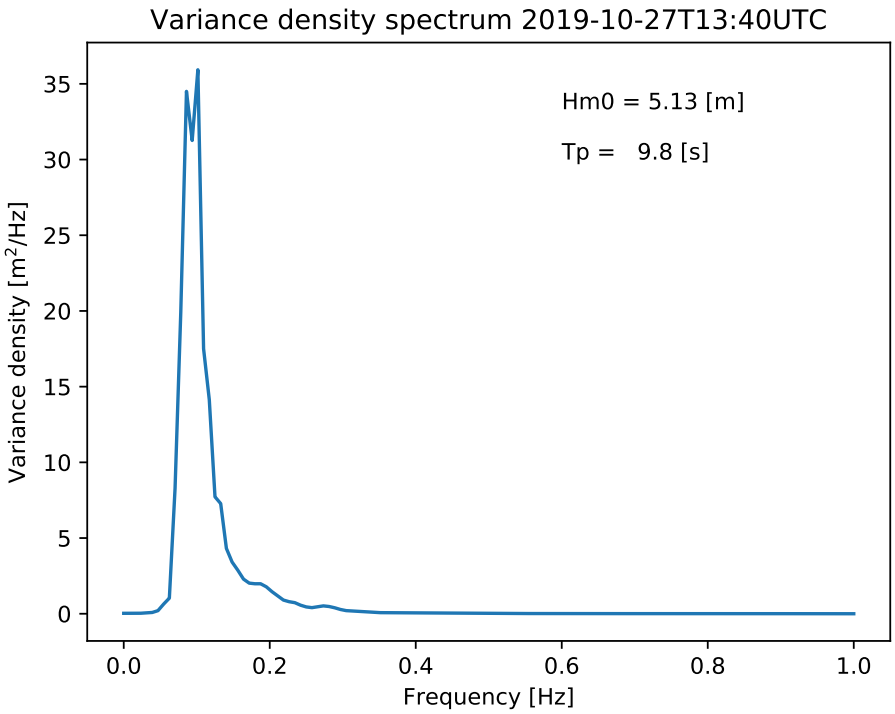

Figure 3.5: The variance density spectrum of the time series in Fig 3.3.

any further ado and no interaction will take place (we'll see later that this is a half-truth). Each frequency band accounts for a certain amount of the variance, hence the variance of all the frequency bands must equal the total variance,

$$\{\eta^2\} = \frac{1}{2}\sum_{k=0}^{N} a_k^2 = \sum_{k=0}^{N/2} F_k \Delta f_k. \tag{3.2.5}$$

As $\Delta f \to 0$, the summation (3.2.5) approaches the integral

$$\{\eta^2\} = \int_0^\infty F(f)\,\mathrm{d}f. \tag{3.2.6}$$

3.2.1 Spectral moments and integrated parameters

The second method for computing the wave height is the spectral estimate

$$H_{m_0} = 4\sqrt{E}. \tag{3.2.7}$$

The reason it is given this strange subscript is that the spectral "moment" of order n is defined as

$$m_n \equiv \int_0^\infty f^n F(f)\,\mathrm{d}f. \tag{3.2.8}$$

The zeroth moment m_0 is then simply the integral E of the variance density spectrum (3.2.6), which we know from Eq (3.2.5) is the total wave variance. Its square root multiplied by 4 is then "4 rms".

3.3 Wave energy balance equation

The spectral representation and the superposition principle allows us to treat the water surface as a sum of (weakly interacting, more later) Fourier components, each advancing with a phase speed given by the dispersion relation (2.1.11) and whose energy advances with the group speed (2.2.4). This means that we can see the wave energy balance as an advection equation (cf. Sec. A.2),

$$\frac{\partial F}{\partial t} + \boldsymbol{\nabla}\cdot(\boldsymbol{c}_\mathrm{g} F) = S_\mathrm{in} + S_\mathrm{ds} + S_\mathrm{nl}. \tag{3.3.1}$$

Here S_in is an *input* source term that describes wave growth, S_ds is a *dissipation* source term that describes energy loss by white-capping etc., and S_nl is a source term that describes *nonlinear* wave-wave interactions and transfer of energy between different wave components.

3.3.1 Source terms

This equation is immensely important in wave modelling. It is at the heart of every spectral wave model. The variance (often referred to as energy) density is a function $F = F(x, y, t, f, \theta)$. So it varies with location, time, frequency f and *direction of propagation* θ. Note also that although we refer to it as the energy balance equation, the energy density is strictly speaking $\rho g F$. To see this, start with a single sine wave and add the potential and kinetic energy, Eqs (2.2.1)+(2.2.2) = $\rho g a^2/2 = \rho g F \Delta f$. The latter is known from Eq (3.2.4).

Temporarily setting the source terms on the righthand-side of (3.3.1) to zero (hence implying no wind input, no wave breaking and no nonlinear interaction between the wave components), we see that the left hand side is simply an advection balance, that is, the amount of wave energy that comes rolling in on the group velocity minus the amount the goes out (this is what the divergence operator calculates) must equal the local rate of change of wave energy density. In other words, if more energy enters than leaves, the energy level must go up. The right hand side is where the physics lies. The source terms represent wind input (in), dissipation through wave breaking (white capping) and other processes (ds) and nonlinear interaction between Fourier components (nl). This is where the weak interaction comes in. If surface waves were perfectly linear this term would not exist. Then various Fourier components would travel across the ocean, completely oblivious of other wave components. This is not the case, however, and waves do interact, albeit very weakly. This weak interaction is all the same enough to cause wave energy to "propagate" in the spectrum toward lower and higher frequencies, away from the central area (the peak frequency) where the wind feeds energy into the wave field (parameterized here through S_{in}). For a more detailed description of the source terms, see for example Holthuijsen (2007).

3.4 Wave action

If the wave is riding on a current, the *Doppler effect* will lead an observer standing on the shore to see a different frequency $\omega = \sigma + \boldsymbol{k} \cdot \boldsymbol{u}$. Here, $\sigma = 2\pi f$ is the *intrinsic* circular frequency which an observer riding on the current would observe. This invalidates Eq (3.3.1). Wave energy is not conserved in the presence of a slowly changing current because energy is transferred between the wave field

and the mean current. Fortunately, the *wave action density*

$$N \equiv F/\sigma \tag{3.4.1}$$

does what the wave energy density cannot: it is conserved in the presence of currents,

$$\frac{\partial N}{\partial t} + \boldsymbol{\nabla} \cdot ((\boldsymbol{c}_\mathrm{g} + \boldsymbol{u})N) = 0 \tag{3.4.2}$$

(again in the absence of source terms). The wave action has a number of interesting properties and is reminiscent of the Planck constant in quantum physics. The energy density is proportional to $F = \sigma N$—this can be seen from the definition (3.4.1). We now make a statement which we will prove over the following two sections: The wave pseudo-momentum density is proportional to

$$\frac{F}{c} = \frac{Fk}{\omega} = Nk. \tag{3.4.3}$$

Here we have reverted to using $\omega = 2\pi f$ because we assume zero currents, in which case $\sigma = \omega$.

The action balance equation Eq (3.4.2) with source terms is written

$$\frac{\partial N}{\partial t} + \boldsymbol{\nabla} \cdot ((\boldsymbol{c}_\mathrm{g} + \boldsymbol{u})N) = \sum_i S_i/\omega. \tag{3.4.4}$$

If we now multiply Eq (3.4.4) by $\rho g k$ and integrate it we get

$$\rho g \int_0^\infty \frac{\partial (Nk)}{\partial t}\,\mathrm{d}\omega + \rho g \int_0^\infty \boldsymbol{\nabla} \cdot ((\boldsymbol{c}_\mathrm{g} + \boldsymbol{u})Nk)\,\mathrm{d}\omega = \rho g \sum_i \int_0^\infty \frac{k}{\omega} S_i\,\mathrm{d}\omega. \tag{3.4.5}$$

Here, the i sums over the different source terms.

The relation between the wave momentum as defined through the Stokes drift in (2.2) and our definition of wave momentum here is best explained as follows. The Stokes transport equals the mean wave momentum, as shown in Eq (2.2.12). For a single sine wave in intermediate water depth (Phillips, 1977), the Stokes drift is

$$u_\mathrm{S}(z) = a^2 \omega k \frac{\cosh(2k(z+h))}{2\sinh^2(kh)}, \tag{3.4.6}$$

where h is the water depth. In deep water, where the general dispersion relation reduces to (2.1.11), that is where $\omega^2 = gk\tanh kh \approx gk$ when $kh \to \infty$ (short waves in deep water), this simplifies to

$$u_{\mathrm{S}}(z) = \omega k a^2 \mathrm{e}^{2kz}. \tag{3.4.7}$$

Since the amplitude is related to the spectrum as $a^2/2 = F(\omega)\mathrm{d}\omega$, we see that the Stokes drift of a spectrum of deep-water waves is

$$u_{\mathrm{S}}(z) = 2\int_0^\infty \omega k \mathrm{e}^{2kz} F(\omega)\,\mathrm{d}\omega. \tag{3.4.8}$$

The *Stokes transport* is the vertical integral of the Stokes drift,

$$U_{\mathrm{S}} = 2\int_{-\infty}^0 \int_0^\infty k\omega \mathrm{e}^{2kz} F(\omega)\,\mathrm{d}\omega\,\mathrm{d}z = \int_0^\infty \omega F(\omega)\,\mathrm{d}\omega. \tag{3.4.9}$$

Substituting $\omega = gk/\omega$ for deep-water waves (2.1.11), we can now write

$$U_{\mathrm{S}} = g\int_0^\infty \frac{k}{\omega} F(\omega)\,\mathrm{d}\omega. \tag{3.4.10}$$

We now finally get to the end of this by noting that the wave momentum defined in Eq (2.2.12) is

$$M_{\mathrm{w}} = \rho U_{\mathrm{S}} = \rho g\int_0^\infty \frac{k}{\omega} F(\omega)\,\mathrm{d}\omega. \tag{3.4.11}$$

Chapter 4

Air-sea fluxes

In this chapter we discuss the air-sea fluxes of mass, momentum and energy, briefly describing common parameterisations. More importantly, we connect the air-sea momentum and energy fluxes to the surface waves dynamics and the two-dimensional wave spectrum described in the previous chapter.

4.1 Air-sea fluxes

The air-sea interface controls the transfer of matter, momentum and energy between the atmosphere and the ocean. This includes the transfer of heat, momentum, salt (freshwater), trace gases (e.g. CO_2), between the ocean and atmosphere. The rate per unit area of these elements is termed *flux*. With regards to the air-sea interface there are two primary distinctions for types of flux: radiative and turbulent.

4.1.1 Radiative flux

Radiative fluxes are the absorption and emittance of electromagnetic (EM) radiation and only contribute to the heat flux. There are two prominent bands of EM radiation for air-sea interaction: shortwave (SW), which is the visible band originating from the sun, and longwave (LW), which is the infrared band that is emitted by clouds and the ocean interface. The two bands are absorbed very differently by the ocean with LW mostly being absorbed in the upper mm while SW can penetrate on the order of 100 m depending on the biology.

The net heat flux is the sum of the radiative fluxes and two other sources which will vary with turbulent processes: sensible heat (due to temperature difference between ocean and atmosphere) and latent heat (due to evaporation). The net heat flux is given by the equation

$$Q_{\mathrm{net}} = Q_{\mathrm{SW}} + Q_{\mathrm{LW}} + Q_{\mathrm{SH}} + Q_{\mathrm{LH}}, \tag{4.1.1}$$

where Q_{SW} is the net shortwave radiation, Q_{LW} is the net longwave radiation, Q_{SH} is the net sensible heat, and Q_{LH} is the net latent heat.

The net shortwave is the difference between the downwelling and upwelling SW radiation,

$$\begin{aligned} Q_{\mathrm{SW}} &= Q_{\mathrm{SW}}\downarrow - Q_{\mathrm{SW}}\uparrow \\ &= (1-\alpha)\, Q_{\mathrm{SW}}\downarrow, \end{aligned} \tag{4.1.2}$$

where α is the albedo defined as $Q_{\mathrm{SW}}\uparrow / Q_{\mathrm{SW}}\downarrow$.

$$\begin{aligned} Q_{\mathrm{LW}} &= Q_{\mathrm{LW}}\downarrow - Q_{\mathrm{LW}}\uparrow \\ &= Q_{\mathrm{LW}}\downarrow - \epsilon_{\mathrm{LW}}\sigma_{\mathrm{SB}}T_{\mathrm{s}}^4 - (1-\epsilon_{\mathrm{LW}})\, Q_{\mathrm{LW}}\downarrow \\ &= \epsilon_{\mathrm{LW}}\left(Q_{\mathrm{LW}}\downarrow - \sigma_{\mathrm{SB}}T_{\mathrm{s}}^4\right), \end{aligned} \tag{4.1.3}$$

where ϵ_{LW} is the LW surface emissivity ($\epsilon_{\mathrm{LW}} = 1$ for black-body emission), $\sigma_{\mathrm{SB}} = 5.67 \times 10^{-8}$ W m^{-2} K^{-4} is the Stefan-Boltzmann constant, and T_{s} is the surface (skin) temperature, which is generally slightly cooler than the bulk fluid beneath.

4.1.2 Turbulent flux

Turbulent fluxes are, as the name suggests, fluxes which are controlled by turbulent processes. Turbulent processes are important for the transfer of matter, momentum and energy. Air-sea fluxes we are focused on the vertical transport and these are calculated from the correlation of the property (e.g. heat, momentum, gas concentration) and the vertical velocity. This becomes,

$$\begin{aligned} \Phi_x &= \langle(\bar{x}+x')(\bar{w}+w')\rangle, \\ &= \langle\bar{x}\bar{w} + x'\bar{w} + \bar{x}w' + x'w'\rangle, \\ &= \langle x'w'\rangle, \end{aligned} \tag{4.1.4}$$

where Φ_x is the flux, $\bar{x}$ and x' are the mean and variable components of the property and $\bar{w}$ and w' are the mean and variable components of the vertical velocity. By definition $\langle x'\rangle = \langle w'\rangle = 0$ and assuming the mean vertical velocity is 0 ($\bar{w} = 0$) then it is easy to show that only the turbulent components are important.

Figure 4.1 shows two timeseries with zero mean to represent two turbulent signals. They are positively correlated so the associated flux would be positive. There can exist large spikes in the *instantaneous* flux that are significantly larger than the mean flux. This is referred to as *intermittency*, which is related to the statistical distribution of the turbulent fluctuations.

So, the turbulent fluxes in the vertical direction for momentum, sensible heat, and

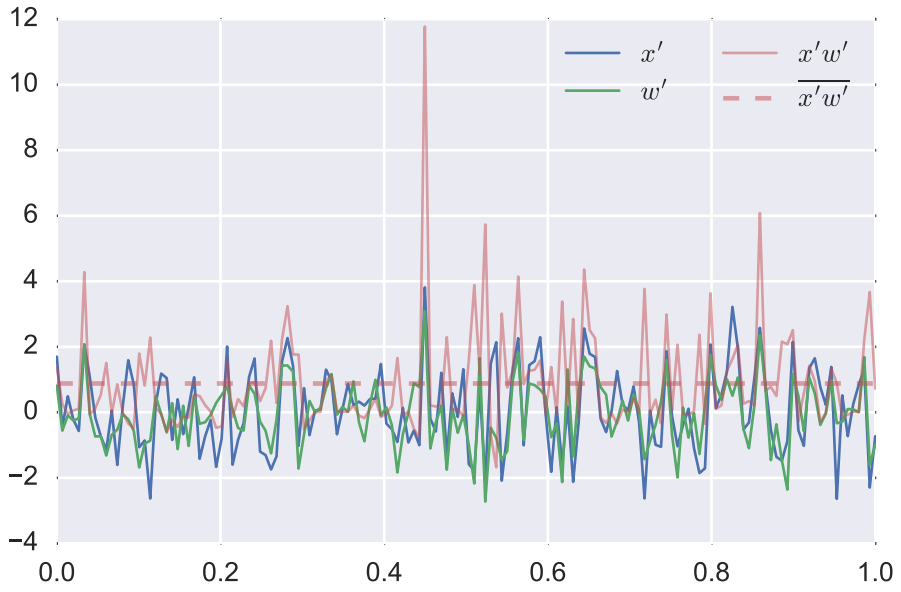

Figure 4.1: Sample turbulent time series and their correlation.

latent heat are

$$\tau_x = \rho_\mathrm{a}\overline{u'w'} \tag{4.1.5}$$

$$\tau_y = \rho_\mathrm{a}\overline{v'w'} \tag{4.1.6}$$

$$Q_\mathrm{SH} = \rho_\mathrm{a}c_\mathrm{P}\overline{\theta'w'} \tag{4.1.7}$$

$$Q_\mathrm{LH} = \rho_\mathrm{a}L_\mathrm{E}\overline{q'w'}. \tag{4.1.8}$$

where ρ_a is the air density, c_P is the specific heat of air at constant pressure, and L_E is the latent heat of vaporization.

These fluxes, if measured directly (more on that in a bit), are measured on the air-side of the air-sea interface and are assumed to be horizontally homogeneous (i.e. turbulence statistics do not vary locally) and are continuous across the air-sea interface. As the horizontally homogeneous assumption is with regards to turbulence statistics this is generally valid in the ocean. The continuity assumption is also generally valid, with the exception of the momentum flux as surface gravity waves can influence the momentum balance between the ocean and atmosphere. In general, waves are in equilibrium with the momentum stress in the atmosphere and ocean (i.e. wave growth = wave dissipation), but there are a few instances,

such as when waves are growing or swell propagation with no wind, that the waves are either a net sink or source of momentum respectively.

4.1.3 Bulk flux parameterizations

There are many challenges to directly measuring turbulent fluxes out at sea, and such observations are, therefore, relatively rare. Amongst the many challenges are having instruments with sufficient accuracy and precision to detect the turbulent components of a given signal. Due to the increased resolution of the measurements, other sources of noise, e.g. most notably flow distortion from the instrument platform, must be accounted for. While such measurements are invaluable for studying air-sea interaction, they are ultimately of limited use for many applications, most notably for ocean forecasting/prediction that do not directly solve the turbulent components of the physical fields. It is, therefore, practical to look for parameterizations for the turbulent fluxes using the mean values as these mean values are easier to measure and can also be resolved by numerical models. These parameterizations are called "bulk flux" parameterizations as they relate turbulent processes with mean values of the bulk of the fluid. These parameterizations are very important for climate modeling as uncertainties can accumulate to large levels over climactic time scales.

At its simplest, we approximate the turbulent transfer using the associated mean values, i.e.

$$\overline{w'x'} = c_x^{1/2} c_{\mathrm{d}}^{1/2} S \Delta X, \tag{4.1.9}$$

where x' is any turbulent quantity as mentioned previously, c_x is the transfer coefficient for the quantity x', c_{d} is momentum transfer, and ΔX is the difference in the mean quantities of X across the air-sea interface. Often c_x and c_{d} are combined to make a single turbulent transfer coefficient. The scale S denotes the scalar difference in velocity across the air-sea interface

$$S^2 = (\bar{u}_{\mathrm{a}} - \bar{u}_{\mathrm{o}})^2 + (\bar{v}_{\mathrm{a}} - \bar{v}_{\mathrm{o}})^2 + u_{\mathrm{g}}^2, \tag{4.1.10}$$

where the subscripts a and o denote the atmosphere and ocean respectively. In Eq. (4.1.10) u_{g} is a “gustiness” factor is added in order to have non-zero momentum fluxes at low winds by parameterizing the effect of convection on momentum transfer. Ths gustiness parameter is typically related to atmospheric stability and a linear function of the convective velocity scale.

The classical form of the bulk fluxes for momentum, sensible heat and latent heat

of vaporization are

$$\tau_x = \rho_{\mathrm{a}} c_{\mathrm{d}} S \Delta \bar{u}, \tag{4.1.11}$$
$$\tau_y = \rho_{\mathrm{a}} c_{\mathrm{d}} S \Delta \bar{v}, \tag{4.1.12}$$
$$Q_{SH} = \rho_{\mathrm{a}} c_{\mathrm{P}} c_{\mathrm{h}} S \Delta \theta, \tag{4.1.13}$$
$$Q_{LH} = \rho_{\mathrm{a}} L_{\mathrm{E}} c_{\mathrm{e}} S \Delta q, \tag{4.1.14}$$

where Δ denotes the difference across the air-sea interface, ρ_a is the air density, c_P is the specific heat of air at constant pressure, L is the latent heat of vaporization and c_d, c_h and c_e are the turbulent transfer coefficients for momentum, sensible heat and latent heat of vaporization. Equations (4.1.11)-(4.1.14) are sometimes also written in terms of the "turbulent scale value", which is denoted by a $*$ subscript, i.e.

$$\tau_x = \rho u_*^2 \Delta \bar{u} / S, \tag{4.1.15}$$
$$\tau_y = \rho u_*^2 \Delta \bar{v} / S, \tag{4.1.16}$$
$$Q_{\mathrm{SH}} = \rho c_{\mathrm{P}} u_* \theta_*, \tag{4.1.17}$$
$$Q_{\mathrm{LH}} = \rho L_{\mathrm{E}} u_* q_*. \tag{4.1.18}$$

4.1.4 Turbulent transfer coefficients

The key components in determining the turbulent transfer coefficient are the height in the boundary layer where the bulk measurements are made z, the roughness length of the the air-sea interface z_0 and the stability of the atmospheric boundary layer $\Phi_x(z/L)$ where L is the Obukhov length scale (L is the level where convective and shear forcing are similar). The stability function and Obukhov length will be described in more detail in Chapter 5. For the general form of Eq. (4.1.9), the transfer coefficient is

$$c_x^{1/2} = \frac{\kappa}{\ln\left(z/z_{0x}\right) - \Phi_x\left(z/L\right)}, \tag{4.1.19}$$

where κ is the von Kármán constant and is typically about 0.40. Equation (4.1.19) assumes that under neutral stability (i.e. no convection or stratification) the the turbulent velocity has a logarithmic profile, also referred to as "law of the wall", at the height of the bulk measurements. Also, in (4.1.19) the roughness length z_{0x} will be different for momentum, sensible heat, etc. Therefore, we can write the

turbulent transfer coefficients as

$$c_{\mathrm{d}} = \left(\frac{\kappa}{\ln\left(z/z_{0u}\right) + \Phi_u\left(z/L\right)} \right)^2, \tag{4.1.20}$$

$$c_{\mathrm{h}} = \left(\frac{\kappa}{\ln\left(z/z_{0u}\right) + \Phi_u\left(z/L\right)} \right) \left(\frac{\kappa}{\ln\left(z/z_{0t}\right) + \Phi_{\mathrm{h}}\left(z/L\right)} \right), \tag{4.1.21}$$

$$c_{\mathrm{e}} = \left(\frac{\kappa}{\ln\left(z/z_{0u}\right) + \Phi_u\left(z/L\right)} \right) \left(\frac{\kappa}{\ln\left(z/z_{0q}\right) + \Phi_q\left(z/L\right)} \right), \tag{4.1.22}$$

where the subscripts u, t and q denote momentum, sensible heat and latent heat.

4.2 Wave-induced momentum and energy fluxes

Breaking waves inject turbulence kinetic energy into the ocean, and parameterizations of this effect can be found in e.g. Gemmrich et al. (1994) and Craig and Banner (1994). With some variations, in both cases the flux is made dependent on the friction velocity u_*, but ultimately the energy flux into the ocean is by way of the wave field. Since surface waves possess mean momentum (represented by the Stokes transport), they also influence the air-sea momentum fluxes. We will briefly describe the sea state dependent momentum and energy fluxes for the case of a two-dimensional spectral representation of the wave field.

The total atmospheric flux of momentum, here denoted $\boldsymbol{\tau}_{\mathrm{a}}$, is responsible both for wave growth and also for accelerating the upper ocean mean currents through turbulent drag. Thus we introduce the partition

$$\boldsymbol{\tau}_{\mathrm{a}} = \boldsymbol{\tau}_{\mathrm{ao}} + \boldsymbol{\tau}_{\mathrm{aw}}, \tag{4.2.1}$$

where $\boldsymbol{\tau}_{\mathrm{ao}}$ represents the direct acceleration of the mean Eulerian currents and $\boldsymbol{\tau}_{\mathrm{aw}}$ represents the momentum flux into the wave field. As demonstrated by Longuet-Higgins (1953), dissipation of the waves is associated with a momentum flux from the waves to the mean Eulerian current, which is usually referred to as the 'virtual wave stress' (Longuet-Higgins, 1969; Weber, 2001). We denote this momentum flux $\boldsymbol{\tau}_{\mathrm{wo}}$. The total flux of momentum into the mean Eulerian current, here denoted $\boldsymbol{\tau}_{\mathrm{o}}$, consequently has two sources:

$$\boldsymbol{\tau}_{\mathrm{o}} = \boldsymbol{\tau}_{\mathrm{ao}} + \boldsymbol{\tau}_{\mathrm{wo}}, \tag{4.2.2}$$

that is, both the direct forcing by turbulent drag and the transfer of momentum from dissipating waves. This partitioning of the momentum fluxes between the atmosphere, the waves, and the Eulerian mean current is illustrated in Figure 4.2.

The equation for conservation of mean wave momentum is (Weber et al., 2006)

$$\frac{\partial \boldsymbol{M}_{\mathrm{w}}}{\partial t} + \nabla_h \cdot \mathcal{F}_{\mathrm{w}} = \boldsymbol{\tau}_{\mathrm{aw}} - \boldsymbol{\tau}_{\mathrm{wo}}. \tag{4.2.3}$$

Here $\mathcal{F}_{\mathrm{w}}$ represents the advection of mean wave momentum by the group velocity $\boldsymbol{c}_g$, i.e. for a monochromatic wave we have $\mathcal{F}_{\mathrm{w}} = \boldsymbol{c}_g \boldsymbol{M}_{\mathrm{w}}$. Equation (4.2.3) is a variant of the wave action equation (3.4.4), which is solved by numerical wave prediction models. If the total atmospheric flux $\boldsymbol{\tau}_{\mathrm{a}}$ and the wave field is know,

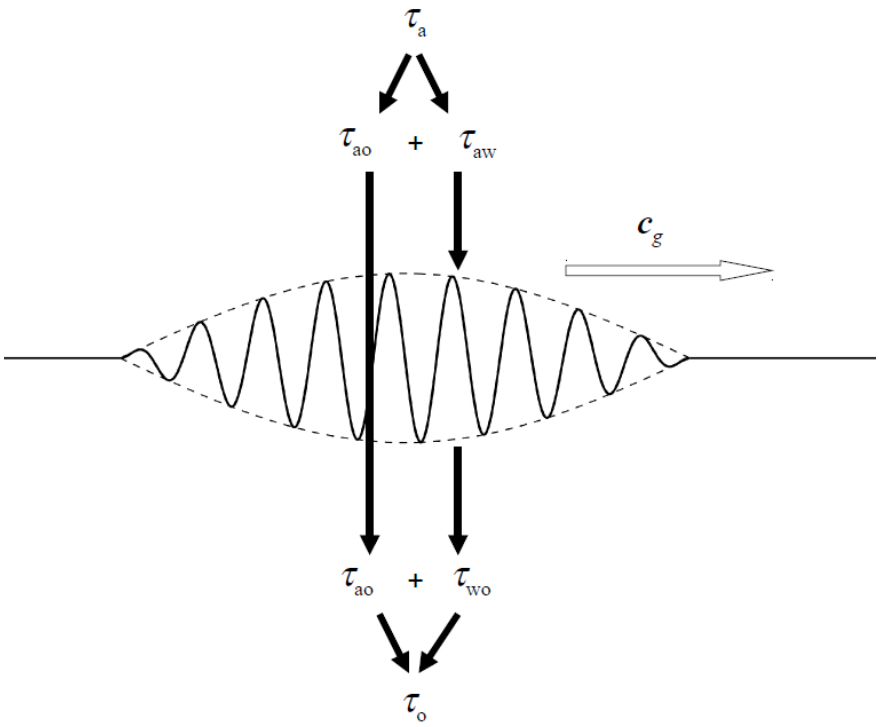

Figure 4.2: Partitioning of momentum fluxes for the case of deep water waves. The nomenclature of the subscripts is 'a'—total flux from the atmosphere, 'ao'—atmosphere to ocean, 'aw'—atmosphere to waves, 'wo'—waves to ocean, 'o'—total momentum flux into the ocean. The momentum flux from the atmosphere to the waves may very well be negative, for example swell driven wind, the main point is that the total momentum of the atmosphere-wave-ocean system must be conserved.

Eqs. (4.2.1), (4.2.2) and (4.2.3) can be combined to yield the effective stress into the ocean:

$$\boldsymbol{\tau}_{\mathrm{o}} = \boldsymbol{\tau}_{\mathrm{a}} - \frac{\partial \boldsymbol{M}_{\mathrm{w}}}{\partial t} - \nabla_{\mathrm{h}} \cdot \mathcal{F}_{\mathrm{w}}. \tag{4.2.4}$$

If we integrate the momentum density defined in Section 3.1, Eq (3.4.3), now dropping the "pseudo" warning, and multiply by ρg we get

$$\boldsymbol{M}_{\mathrm{w}} \equiv \rho g \int_0^\infty \frac{\boldsymbol{k}}{\omega} F(\omega)\, \mathrm{d}\omega = \rho g \int_0^\infty \boldsymbol{k} N(\omega)\, \mathrm{d}\omega, \tag{4.2.5}$$

which has units $[\mathrm{kg\,m\,s^{-1}\,m^{-2}}]$, ie, momentum per area. This is the *spectral representation* of the wave momentum in Eq (2.2.12). The momentum fluxes into the ocean, which drive the mean oceanic flows, can thus be expressed in terms of the source functions in the wave action balance equation. The flux of turbulence kinetic energy due to breaking waves can also be expressed in terms of the source functions.

In coupled wave-ocean modeling systems we can exploit this dependence and let the wave model communicate sea state dependent fluxes to the ocean model, calculated from numerical integration of the time dependent source terms. One caveat here is that numerical wave models have a spectral cutoff. The highest frequency such models resolve is typically around 0.5 Hz, or a wave cutoff frequency ω_c of about 12.5 rad/s. Janssen (2012) argues that the total fluxes from the atmosphere are quite well known, and hence we only need a quantification of the difference between what *goes into* and what *comes out* of the waves. Furthermore, it is implicitly assumed that there is a balance between input and dissipation in the diagnostic part of the wave spectrum ($\omega > \omega_c$). For the momentum flux into the ocean we then have[1]

$$\boldsymbol{\tau}_{\mathrm{o}} = \boldsymbol{\tau}_{\mathrm{a}} - \rho g \int_0^{w_c} \frac{\boldsymbol{k}}{\omega} \left(S_{\mathrm{in}} + S_{\mathrm{ds}}\right) \mathrm{d}\omega. \tag{4.2.6}$$

Similarly, if we define the total energy flux from the atmosphere as Φ_{a}, we can express the energy flux into the ocean as

$$\Phi_{\mathrm{o}} = \Phi_{\mathrm{a}} - \rho g \int_0^{w_c} \left(S_{\mathrm{in}} + S_{\mathrm{ds}}\right) \mathrm{d}\omega. \tag{4.2.7}$$

[1]The dissipation source term S_{ds} is by convention defined such that it is always negative.

Chapter 5

Upper ocean turbulence

The turbulence in the upper part of the ocean is, directly or indirectly, generated by wind and waves. Turbulence is suppressed by stable stratification, hence the air-sea heat and mass fluxes play an important role. Numerical ocean circulation models contain parameterizations of the oceanic turbulence, which is used to assess the effective eddy viscosity and eddy diffusivities that influence the mean velocities and average salinity and temperature profiles. This chapter provides an overview of two commonly used parameterizations.

5.1 The role of stratification

Vertical mixing of stratified fluids raises the potential energy, and therefore requires mechanical energy. One source of mechanical energy is due to instabilities associated with velocity shear. In the ocean the vertical shear dominates over horizontal shear, and the shear production is typically represented by

$$S^2 = (\partial \bar{\boldsymbol{u}}/\partial z)^2. \tag{5.1.1}$$

Buoyancy is represented by the buoyancy frequency, or the Brunt-Väisälä frequency as it is often called:

$$N^2 = -\frac{g}{\rho_0}\frac{\partial \rho}{\partial z}. \tag{5.1.2}$$

The Richardson number[1], Ri, is a nondimensional quantity that expresses the relative importance of TKE suppression by buoyancy and TKE production by the shear flow:

$$\mathrm{Ri} = \frac{N^2}{S^2}. \tag{5.1.3}$$

For Ri < 0, the fluid is statically unstable, while for Ri > 0, the fluid is statically stable. As the value decreases so that Ri < 0.25, buoyancy will typically be unable to suppress shear production, and mechanical mixing will start to homogenize the fluid.

In the ocean, the necessary mechanical energy comes from wind and waves. Simple models for how a wind-mixed, turbulent surface layer entrains into a stratified fluid can be derived using energy considerations and dimensional analysis. Here we will follow Turner and Kraus (1967) and consider a situation as depicted in Fig. 5.1. At the surface there is a constant wind stress τ with an associated friction velocity $u_* = \sqrt{\tau/\rho_0}$. The surface layer has density $\rho_1 = \rho_0 - \Delta\rho$, and a

[1] The specific form shown here is typically referred to as the *gradient* Richardson number.

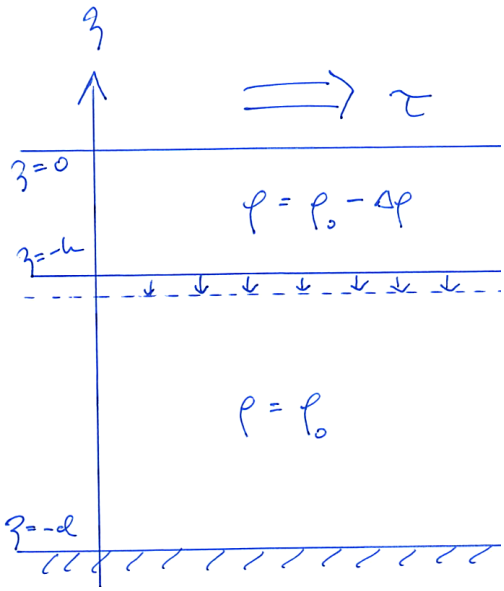

Figure 5.1: A two-layer model for the entrainment of a turbulent surface layer into the denser water masses of the ocean interior.

thickness h. The total water depth is d. The question now is how fast the surface layer entrains into the layer below, that is, what is $v = dh/dt$? Turner and Kraus (1967) consider three cases, briefly summarized below.

In the first case it is assumed that the density difference $\Delta\rho$ is negligible. Then the only velocity scale is u_*, hence the entrainment velocity v must be proportional to the friction velocity. In the second case, buoyancy effects are assumed to totally dominate at the smallest scales. Returning to the Kolmogorov microscales from Sec. 1.2.2, we require for the accelerations (buoyancy vs. the smallest turbulent eddies) that

$$\frac{g\Delta\rho}{\rho_0} \gg \frac{l_K}{t_K^2} = \left(\frac{\epsilon^3}{\nu}\right)^{\frac{1}{4}}.$$

The small scale turbulence is very efficiently damped out, and entrainment is caused by "large eddies sweeping away the viscous boundary at the interface", to use their own description. In the third, intermediate case we need to employ energy considerations. First of all we note that since the total mass is conserved, we will have

$$\rho_1 h + (d-h)\rho_0 = \text{const.}, \tag{5.1.4}$$

which implies that $h\Delta\rho$ is also constant. Secondly, we calculate the potential energy E_p:

$$E_{\mathrm{p}} = \int_{-d}^{0} \rho g z \, \mathrm{d}z = \frac{1}{2}\Delta\rho g h^2 - \frac{1}{2}\rho_0 g d^2. \tag{5.1.5}$$

Now, from (5.1.4) we obtain that $C = \Delta\rho g h$ is constant. When we take the time derivative of E_p, we therefore find that

$$\frac{\mathrm{d}E_{\mathrm{p}}}{\mathrm{d}t} = \frac{C}{2}\frac{\mathrm{d}h}{\mathrm{d}t} = \frac{1}{2}Cv. \tag{5.1.6}$$

If the wind energy input is constant, and all the mechanical energy is used to increase the potential energy by mixing, then it follows from (5.1.6) that the entrainment velocity v is constant, and that the thickness of the surface layer increases linearly in time. Turner and Kraus (1967) goes on to introduce the Richardson number, which in this case becomes

$$\mathrm{Ri} = \frac{(g\Delta\rho/\rho_0 h)}{(u_*^2/h^2)}, \tag{5.1.7}$$

and argue on dimensional grounds that we should have $v/u_* = f(\mathrm{Ri})$. For example, Kato and Phillips (1969) found good agreement with $f = 2.5\mathrm{Ri}^{-1}$ in a rather neat experiment involving an annular tank with constant surface stress provided by a rotating disk (see Fig. 5.2).

5.2 Diagnostic turbulence schemes

With diagnostic turbulence schemes we aim to find expressions for the overall effect of the turbulent mixing. Typically these expressions include the eddy viscosity and diffusivity profiles, and also the time dependent surface (or bottom) boundary layer thickness. Such schemes are not formulated as differential equations, but rather as a set of algebraic equations that only require knowledge about the mean flow quantities and the surface (or bottom) fluxes. In ocean models, the diagnostic scheme that is most widely used nowadays is arguably the "*K* profile parameterization" (KPP). The KPP is based on a scheme originally developed for the atmospheric boundary layer, and adapted to the ocean by Large et al. (1994). Their derivation is instructive and based on sound physical reasoning, and below we provide a brief summary of how the scheme is designed (ignoring the bottom boundary layer).

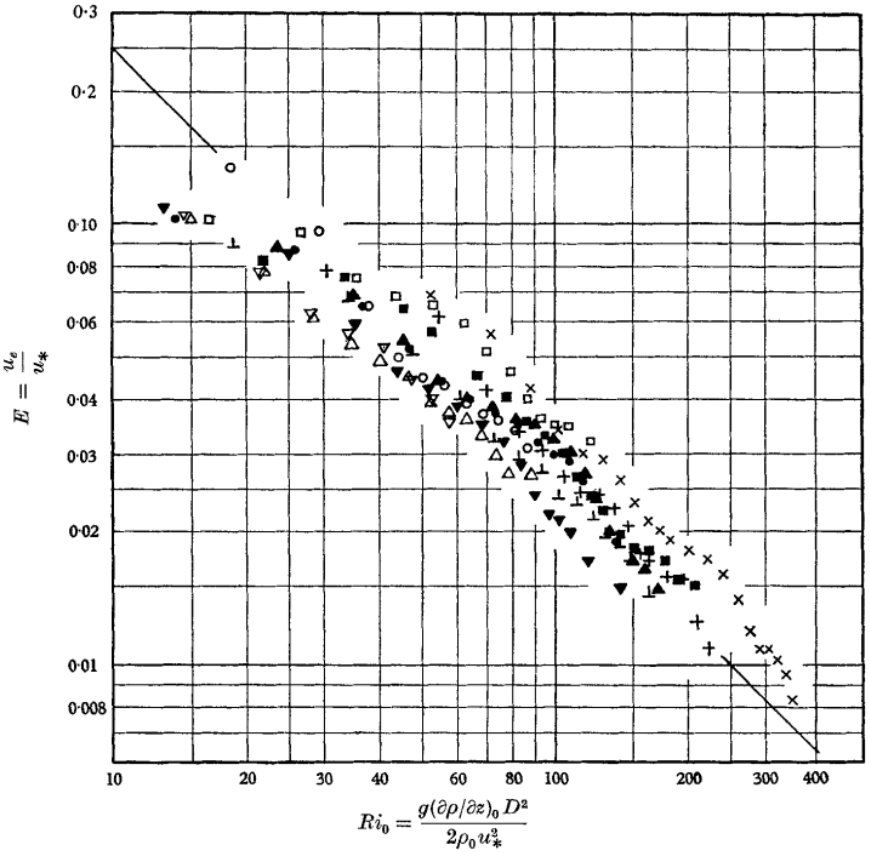

FIGURE 6. The entrainment coefficient E as a function of the overall Richardson number. The parameters represented by the symbols are indicated in the table below:

	$d\rho/dz$ = $1{\cdot}92\times10^{-3}$	$3{\cdot}84\times10^{-3}$	$7{\cdot}69\times10^{-3}$ c.g.s.
τ_0 = 0·995 c.g.s.	□	■	×
1·485	△	▲	
2·12	○	●	+
2·75	▽	▼	⊥

Figure 5.2: Nondimensional entrainment velocity as a function of Richardson number. From the experiments of Kato and Phillips (1969), demonstrating a functional relationship $v/u_* = 2.5\mathrm{Ri}^{-1}$. *Note that the motion is started from rest and the density gradient is initially constant throughout the fluid, which is not the same situation as the one depicted in Fig. 5.1.*

With the KPP scheme we determine the boundary layer depth, h, defined as the limit to which the boundary layer eddies can penetrate in the vertical. Other definitions of the boundary layer thickness exist that are more commonly used, but we will stick to h in this context. Now we need to introduce yet another vertical length scale (and more will come!), namely the Obukhov length[2], L, that was briefly mentioned in Section 4.1.3:

$$L = -\frac{u_*^3}{\kappa B_f}, \tag{5.2.1}$$

where $\kappa = 0.4$ is the von Kármán constant and B_f is the buoyancy flux. A physical interpretation of the Obukhov length is that it represents the depth where turbulence production by the wind-induced shear equals the production by buoyancy. The ratio $|h/L|$ can be used as a measure of the stability of the water column. Small values indicate a stable water column, and as the ratio increases the column can eventually become unstable leading to overturning (e.g. Sutherland et al., 2013).

Next we need to consider the conditions near the surface. In the *Monin-Obukhov similarity theory* (MO theory) it is assumed that the most important quantities here are the distance to the surface, d, the surface flux of momentum, $\boldsymbol{\tau}$, the surface flux of any scalar quantities, $-\overline{w'x'}$, and the buoyancy flux, B_f. The MO theory should be valid in the part of the boundary layer that is closest to the surface, that is, for $d/h < \varepsilon$, where a typical value is $\varepsilon = 0.1$. In addition to the Obukhov length, we use the turbulence parameters u_* and $S_* = -\overline{w'x'}/u_*$. The MO theory now states that there exist universal functions of the nondimensional distance to the surface $\zeta = d/L$:

$$\phi_\mathrm{m}(\zeta) = \frac{\kappa d}{u_*}\frac{\partial|\bar{\boldsymbol{u}}|}{\partial z}, \tag{5.2.2}$$

$$\phi_\mathrm{s}(\zeta) = \frac{\kappa d}{S_*}\frac{\partial\overline{x}}{\partial z}. \tag{5.2.3}$$

These functions can be found empirically and, by integration of (5.2.2) and (5.2.3), used to determine the vertical profiles. Using subscripts "m" and "s" for momen-

[2]Often referred to as the Monin-Obukhov length due to its central place in Monin-Obukhov similarity theory.

tum and scalar quantities, respectively:

$$|\bar{\boldsymbol{u}}| = |\bar{\boldsymbol{u}}_0| + \frac{u_*}{\kappa}\left[\ln\left(\frac{d}{z_\mathrm{m}}\right) + \psi_\mathrm{m}(\zeta)\right], \tag{5.2.4}$$

$$S = S_0 + \frac{S_*}{\kappa}\left[\ln\left(\frac{d}{z_\mathrm{s}}\right) + \psi_\mathrm{s}(\zeta)\right], \tag{5.2.5}$$

where subscript 0 denotes surface values, and the functions ψ_m and ψ_s depend on the stability, being zero for neutral conditions. The values of the roughness lengths z_m and z_s depend on the physical conditions of the surface. The universal functions (5.2.2) and (5.2.3) will be used later on to determine the boundary layer viscosity and diffusivities.

A central part of the KPP scheme is that it allows for non-local transport in the boundary layer. That is, for any quantity x, the vertical turbulent flux is modeled as

$$-\overline{w'x'} = K_x\left(\frac{\partial \overline{x}}{\partial z} - \gamma_x\right). \tag{5.2.6}$$

From this expression we see that the turbulent flux may be nonzero even in the case where we have no vertical gradient in the mean quantity $\overline{x}$. This non-local transport, represented by the term γ_x, can be due to several processes such as convective plumes, Kelvin-Helmholtz instabilities, horizontal roll vortices, and so on. What these processes have in common is that they are typically anisotropic and asymmetric. For example, Langmuir circulation cells are (roughly) aligned with the wind, and convective plumes are typically much more narrow than the compensating return flows.

We define a nondimensional vertical coordinate $\sigma = d/h$ (recall that d is the distance to the surface, which means that $d = -z$ in the ocean), and assign a prescribed vertical shape to the boundary layer diffusivity:

$$K_x(\sigma) = h w_x(\sigma) G(\sigma). \tag{5.2.7}$$

Here w_x is a turbulent vertical velocity scale, and G is a fourth-order polynomial such that the diffusivity and its gradients can be matched to any specific values at the top and bottom of the boundary layer. For $\sigma < \varepsilon$ the MO theory applies, and w_x can be obtained via (5.2.3) and (5.2.6). A continuous turbulent vertical velocity scale w_x, valid throughout the boundary layer, is then

$$w_x(\sigma) = \begin{cases} \frac{\kappa u_*}{\phi_x(\varepsilon h/L)}, & \varepsilon < \sigma < 1, \\ \frac{\kappa u_*}{\phi_x(\sigma h/L)}, & \sigma < \varepsilon. \end{cases} \tag{5.2.8}$$

From these expressions we see that w_x is proportional to u_*. The universal functions are equal to unity for neutral conditions. For stable conditions, we have $\phi_x > 1$, which reduces w_x, and hence directly contributes to reducing the diffusivity value and as a consequence the vertical mixing. For unstable conditions we have the opposite case, with $\phi_x < 1$ and hence enhancement of the vertical mixing. Modifications to these expressions have been suggested, for example to accommodate the effect of Langmuir circulation (McWilliams and Sullivan, 2000).

The time dependent value of h is obtained from the mean velocities and density using a bulk Richardson number:

$$\mathrm{Ri_b} = \frac{(B_\mathrm{r} - B(d))d}{|\bar{\boldsymbol{u}}_\mathrm{r} - \bar{\boldsymbol{u}}(d)|^2 + V_t^2(d)}. \tag{5.2.9}$$

Here subscript r indicates an average value taken in the surface layer ($\sigma < \varepsilon$), and V_t/d represents a turbulent velocity shear that is assumed proportional to the buoyancy frequency N (the full expression is quite complex). The turbulent velocity shear dominates during convection when the mean flow shear is small. The value of h is found as the smallest value of d when $\mathrm{Ri_b}$ becomes equal to a critical value.

Below the boundary layer, the vertical mixing is assumed to result from three processes: (i) resolved vertical shear, (ii) internal wave breaking, and (iii) double diffusion, each process being parameterized as a depth dependent eddy diffusivity. The overall eddy diffusivity is simply the sum of these such that

$$\nu_x(d) = \nu_x^\mathrm{s}(d) + \nu_x^\mathrm{w}(d) + \nu_x^\mathrm{d}(d). \tag{5.2.10}$$

The interior diffusivity and the gradient is matched to the values in the boundary layer. The shear instability term $\nu_x^{\mathrm{us(d)}}$ is taken to be a function of the Richardson number (5.1.3), the internal wave breaking term $\nu_x^w(d)$ is constant, while the double diffusion term $\nu_x^d(d)$ is a function of the density stability ratio, R_ρ:

$$R_\rho = \frac{\alpha(\partial T/\partial z)}{\beta(\partial S/\partial z)}. \tag{5.2.11}$$

Here α is the thermal expansion coefficient and β is the haline contraction coefficient. Efficient numerical implementations of the KPP scheme have been made in community general ocean circulation models such as ROMS and HYCOM, and in one-dimensional column models such as GOTM. The KPP scheme is typically far less computationally costly than the prognostic schemes that we discuss in the next section.

5.3 Prognostic turbulence schemes

One criticism of diagnostic schemes is that they are tuned to perform well for a limited range of environmental conditions, hence the need for turbulence schemes with wider applicability. With commonly used prognostic schemes, we explicitly solve the TKE equation (A.6.2) and derive the eddy viscosity and diffusivities assuming both are proportional to $k^{\frac{1}{2}}l$, with $k = |\boldsymbol{u}'|^2/2$ being the TKE per unit mass and l the length scale of the turbulent eddies. Since we already have the equation governing k, we only need to determine l to close the system of equations. Estimating the length scale is not straightforward, however, and in the so-called "two-equation models" a separate prognostic equation is introduced. This latter equation solves for the time dependent development of l, or some other quantity associated with the turbulence scales.

In Generic Length Scale (GLS) theory (Umlauf and Burchard, 2003), which is commonly applied in modern ocean circulation models (e.g. Warner et al., 2005), a generic parameter ψ is introduced:

$$\psi = (c_\mu^0)^p k^m l^n. \tag{5.3.1}$$

Here c_μ^0 is a stability coefficient, and m, n and p are constants. By adjusting these constants, the generic length scale ψ can take on different forms, and we can recover classic turbulence schemes such as the k-ϵ scheme ($m = 1.5$, $n = -1.0$), the Mellor-Yamada level 2.5 scheme ($m = 1.0$, $n = 1.0$), and the k-ω scheme ($m = 0.5$, $n = -1.0$). In these examples, the generic length scale ψ have units $\mathrm{m}^3/\mathrm{s}^2$, $\mathrm{m}^2/\mathrm{s}^3$, and 1/s, respectively.

Following Umlauf and Burchard (2003), we write the TKE equation as

$$\frac{\mathrm{D}k}{\mathrm{D}t} = \mathcal{D}_k + P + G - \epsilon, \tag{5.3.2}$$

with $\mathcal{D}_k$ representing the transport (diffusive) term, P shear production, G production by buoyancy, and ϵ is the dissipation rate as before. An equation for ψ is formulated on the basis of being dimensionally correct and similar to the equations for ϵ and ω that are used in the k-ϵ and k-ω schemes (not shown here):

$$\frac{\mathrm{D}\psi}{\mathrm{D}t} = \mathcal{D}_\psi + \frac{\psi}{k}\left(c_{\psi 1}P + c_{\psi 3}G - c_{\psi 2}\epsilon\right). \tag{5.3.3}$$

Here the $c_{\psi i}$ are constants and $\mathcal{D}_\psi$ is a transport term equivalent to the one in (5.3.2). The dissipation rate is taken to be

$$\epsilon = (c_\mu^0)^{(3+\frac{p}{n})} k^{(\frac{3}{2}+\frac{m}{n})} \psi^{-(\frac{1}{n})}, \tag{5.3.4}$$

and from this expression we obtain the turbulence length scale as

$$l = (c_\mu^0)^3 k^{\frac{3}{2}} \epsilon^{-1}. \tag{5.3.5}$$

Typical values of the coefficient c_μ^0 are about 0.55, which means that $l \approx 0.17 k^{3/2}/\epsilon$.

We define the eddy viscosity ν_t and the eddy diffusivity κ_t as

$$\nu_t = (k^{\frac{1}{2}} l) S_{\mathrm{M}} + \nu, \tag{5.3.6}$$

$$\kappa_t = (k^{\frac{1}{2}} l) S_{\mathrm{T}} + \kappa, \tag{5.3.7}$$

where ν and κ refer to laminar and molecular values, respectively. The terms S_{M} and S_{T} are typically referred to as stability functions (in some of the literature referred to as "structure functions"). These functions are obtained using so-called Algebraic Reynolds Stress models, in which the Reynolds stresses are explicitly modeled with second-moment closure (e.g. Canuto et al., 2001). The details of these algebraic models are outside the scope of this compendium, but it should be clear at this point that the GLS model contains a number of tunable parameters. In fact, Umlauf and Burchard (2003) argue that each parameter is an independent constraint on the scheme's behaviour, and hence more parameters means that more physically diverse scenarios can be accounted for with the same turbulence scheme. The introduction of the generic length scale, and the parameters m and n, in that sense provide even more flexibility. Umlauf and Burchard (2003) introduce a specific ("generic") parameter set based on a range of numerical experiments representing different types of oceanic flows, in particular an upper ocean boundary layer with turbulence injection from breaking waves.

Introducing two constant turbulent Schmidt numbers $\sigma_k = \nu_t/\kappa_k$ and $\sigma_\psi = \nu_t/\kappa_\psi$, we write the transport terms as

$$\mathcal{D}_k = \frac{\partial}{\partial z}\left(\kappa_k \frac{\partial k}{\partial z}\right), \tag{5.3.8}$$

$$\mathcal{D}_\psi = \frac{\partial}{\partial z}\left(\kappa_\psi \frac{\partial \psi}{\partial z}\right). \tag{5.3.9}$$

The remaining source terms are given by

$$P = \nu_t \left|\frac{\partial \bar{\boldsymbol{u}}}{\partial z}\right|^2, \tag{5.3.10}$$

$$G = -\kappa_t N^2, \tag{5.3.11}$$

where N is the buoyancy frequency as before.

Finally, both k and ψ need boundary conditions at the surface and the bottom. For k a simple no-flux condition at the bottom is applied, and a surface flux condition can accomodate injection of TKE by breaking waves as mentioned in Section 4.2. For the generic length scale ψ it is not so straightforward. One way of implementing boundary conditions is to use (5.3.1) and formulate boundary conditions for the length scale l. Close to the boundaries it is assumed that the length scale is associated with the surface and bottom roughness (see e.g. the implementation by Warner et al., 2005). This method thus requires roughness length estimates. The bottom roughness can be quantified if its physical properties are known (for example sandy vs. rocky bottom), but what values to choose for the case of a wavy boundary layer is unfortunately not so obvious.

Chapter 6

Upper ocean drift currents

While the preceding chapters have dealt with the processes that influence the upper ocean drift velocities, this final chapter focuses on the drift velocities themselves. We briefly review a few simplified models of upper ocean transport, and also look at the wave-induced Coriolis-Stokes force, the possible mechanisms for damping the upper ocean flows, and finally the modeling of buoyant tracers. The latter is particularly relevant to operational oceanography and decision support systems for accidental oil spills and search-and-rescue operations, as well as for the simulation of marine litter transport pathways.

6.1 Wind driven currents

The classic view of wind driven currents is attributed to Ekman (1905) who looked at the response to the wind stress of a rotating ocean. The Ekman response is a balance of the Coriolis term and the wind-induced stress. Assuming a steady state:

$$\frac{1}{\rho}\frac{\partial \tau_x}{\partial z} = -fv, \tag{6.1.1}$$

$$\frac{1}{\rho}\frac{\partial \tau_y}{\partial z} = fu, \tag{6.1.2}$$

where $\tau_{x,y}$ is the stress in the x and y directions, ρ is the water density, and f is the Coriolis paramter. Furthermore, assuming the stress can be expressed using an eddy viscosity

$$\tau_x = A_z \frac{\partial u}{\partial z} \tag{6.1.3}$$

$$\tau_y = A_z \frac{\partial v}{\partial z}, \tag{6.1.4}$$

where A_z is the vertical eddy viscosity. Substituting (6.1.3) and (6.1.4) into (6.1.1) and (6.1.2) and assuming A_z is a constant (as Ekman did) we get two equations which we can solve

$$A_z \frac{\partial^2 u}{\partial z^2} = -fv, \tag{6.1.5}$$

$$A_z \frac{\partial^2 v}{\partial z^2} = fu. \tag{6.1.6}$$

The solution to (6.1.5) and (6.1.6) is

$$u_{\mathrm{E}} = U_0 \cos\left(\frac{\pi}{4} + \frac{z}{\delta_{\mathrm{E}}}\right) \mathrm{e}^{z/\delta_{\mathrm{E}}} \mathrm{sgn}\left(f\right), \tag{6.1.7}$$

$$v_{\mathrm{E}} = U_0 \sin\left(\frac{\pi}{4} + \frac{z}{\delta_{\mathrm{E}}}\right) \mathrm{e}^{z/\delta_{\mathrm{E}}}, \tag{6.1.8}$$

where δ_{E} is the Ekman depth and is given by

$$\delta_{\mathrm{E}} = \left(\frac{A_z}{|f|}\right)^{1/2}, \tag{6.1.9}$$

and U_0 can be calculated by evaluating the surface stress condition, i.e. substituting (6.1.7) and (6.1.8) into (6.1.3) and (6.1.4)

$$U_{\mathrm{o}} = \frac{\sqrt{2}\tau}{\delta_{\mathrm{E}} \rho |f|}. \tag{6.1.10}$$

This solution is the classic "Ekman spiral" where the surface currents are 45° to the right of the wind (left in southern hemisphere) and rotate to the right and decrease exponentially in magnitude with greater depth. The time dependent problem is closely linked to inertial oscillations, which we will discuss more in detail later on (see Fig. 6.1).

Spirals as predicted by Ekman are rarely observed in the ocean. The most likely suspect is the constant eddy viscosity assumption, but others such as the steady wind and homogeneous ocean may also play a role. Observations typically show a smaller deflection at the surface on the order of 10-30° and a more rapid decay and faster rotation with depth, although drifter studies show regional differences, which may be related to differences in stratification (Röhrs and Christensen, 2015).

Another important topic is the Ekman transport, which is the vertically integrated Ekman velocity. By integrating Eqs. (6.1.1) and (6.1.2) from the bottom of the Ekman layer to the surface, it is easy to show that the transport is perpendicular to the wind and is to the right (left) in the northern (southern) hemisphere. It should be noted in particular that the Ekman transport *is independent of* A_z and is only a function of wind stress, density and Coriolis parameter. Coastal upwelling/downwelling are attributed to Ekman transport offshore/onshore due to prevailing winds.

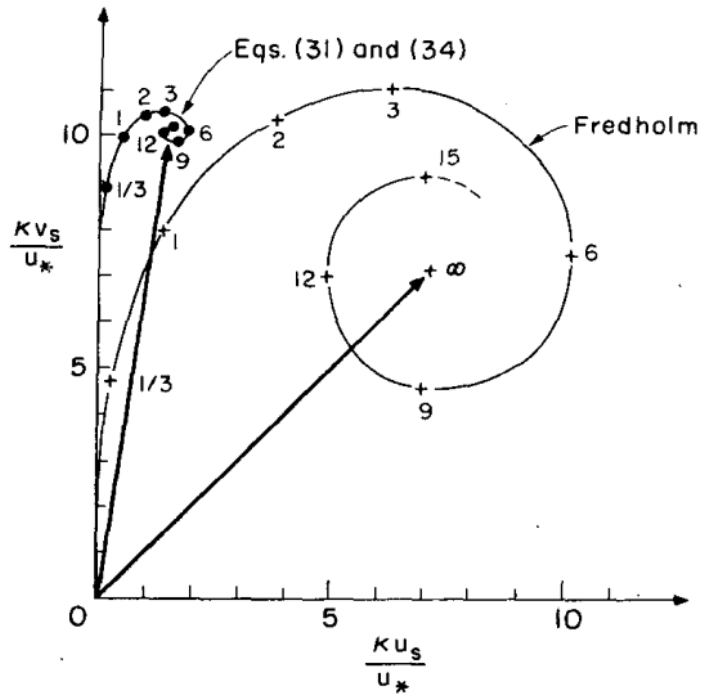

Figure 6.1: Hodographs of the time dependent surface current in Ekman flow. The motion starts from rests and develops in response to a sudden onset of constant wind stress. The "Fredholm" solution assumes a constant eddy and is the one presented in Ekman's original work, while the other is from Madsen (1977), who introduced an eddy viscosity that increases linearly away from the surface. In both cases the surface currents are damped inertial oscillations that tend toward the steady state solution. The eddy viscosity profile used by Madsen yields a smaller angle of deflection between the wind stress and the surface current (from Madsen, 1977, Fig. 2).

6.2 Damped slab models of the upper ocean

In most of the ocean, the vertical structure can typically be described as a well-mixed upper layer—which can range in thickness from meters to hundreds of meters—on top of a stratified deep ocean, with a relatively constant density gradient. Models of the upper ocean which assume constant density are referred to as "slab" models, and have been a popular model for investigating transient currents in the upper ocean (Pollard and Millard, 1970). These models assume that the stress from the wind is transported throughout the mixed layer much faster than timescales associated with acceleration or rotation and hence the ocean can be reasonably be approximated as a slab.

The slab is a 1-D vertical model and assumes the upper ocean is homogeneous in density and velocity (hence the slab). The primary forces are due to acceleration, Coriolis, wind stress and a a dissipative term due to the transfer of energy from the mixed layer to the deep ocean. Parameterizing the loss of energy from the mixed layer to the deep ocean as a linear function of the mixed layer velocity and a damping coefficient r allows for the momentum equations to be written as

$$\frac{\partial u}{\partial t} - fv = \frac{\tau_x}{H\rho} - ru, \tag{6.2.1}$$

$$\frac{\partial v}{\partial t} + fu = \frac{\tau_y}{H\rho} - rv, \tag{6.2.2}$$

where H is the mixed layer thickness. The equations can be simplified further by making use of the complex identities

$$Z = u + \mathrm{i}v, \tag{6.2.3}$$

$$T = \frac{\tau_x + \mathrm{i}\tau_y}{\rho}, \tag{6.2.4}$$

$$\alpha = r + \mathrm{i}f, \tag{6.2.5}$$

so that equations (6.2.1) and (6.2.2) can be written as

$$\frac{\partial Z}{\partial t} + \alpha Z = \frac{T}{H}. \tag{6.2.6}$$

Equation (6.2.6) has some well known properties. For example, with no wind ($T = 0$) the solution is $Z(t) = Z(0)\mathrm{e}^{-\alpha t} = Z(0)\mathrm{e}^{-(\mathrm{i}f+r)t}$ which describes a velocity which rotates clockwise to the right (northern hemisphere) with a frequency

f and the magnitude decays exponentially with a rate r. For a steady wind, such that equation (6.2.6) reaches a steady state, the solution is

$$Z_{\mathrm{E}} = \frac{T}{\alpha H} = \frac{-\mathrm{i}T}{fH\,(1 - \mathrm{i}r/f)}, \tag{6.2.7}$$

which is the mean Ekman velocity in the mixed layer slightly modified by the damping coefficient r. Typically $r/f \ll 1$ and the modification due to the damping coefficient is minimal.

The total current can then be written as the sum of the steady-state current Z_{E} and the time-varying component, which are commonly referred to as *inertial currents*

$$Z_{\mathrm{I}} = Z - Z_{\mathrm{E}}. \tag{6.2.8}$$

Substituting (6.2.8) and(6.2.7) into (6.2.6) gives the equation for the inertial oscillations

$$\begin{aligned} \frac{\partial Z_{\mathrm{I}}}{\partial t} + \alpha Z_{\mathrm{I}} &= -\frac{1}{\alpha}\frac{\partial (T/H)}{\partial t} \\ &= \frac{T}{\alpha H}\left(\frac{1}{H}\frac{\partial H}{\partial t} - \frac{1}{T}\frac{\partial T}{\partial t}\right). \end{aligned} \tag{6.2.9}$$

6.3 The diurnal cycle in the upper ocean

The ocean has a rather large heat capacity and the diurnal range in temperature is modest compared to that of the atmosphere. Nevertheless, when the weather is fair there may be an appreciable impact of the solar heating. In such situations, the wind will typically change from calm in the morning to a fresh breeze during midday, then dropping again in the evening. The combined effects of strong solar forcing and varying winds may lead to a curious diurnal cycle in the upper ocean.

Since the atmosphere is (mostly) transparent to shortwave radiation, the energy is absorbed or reflected at the surface level. Shortwave radiation therefore contributes to *destabilizing* the lower atmosphere, particularly over ground. In contrast, the ocean is almost opaque. The shortwave radiation can, in very clear waters, penetrate to O(100m) depth, although most of the energy is absorbed in the upper few meters. The surface layer heats up and the temperature stratification that develops is *stabilizing*. While the solar forcing suppresses turbulence, wind-induced shear flow produces turbulence, and the structuring of the upper ocean changes throughout the day as these two mechanisms battle for supremacy.

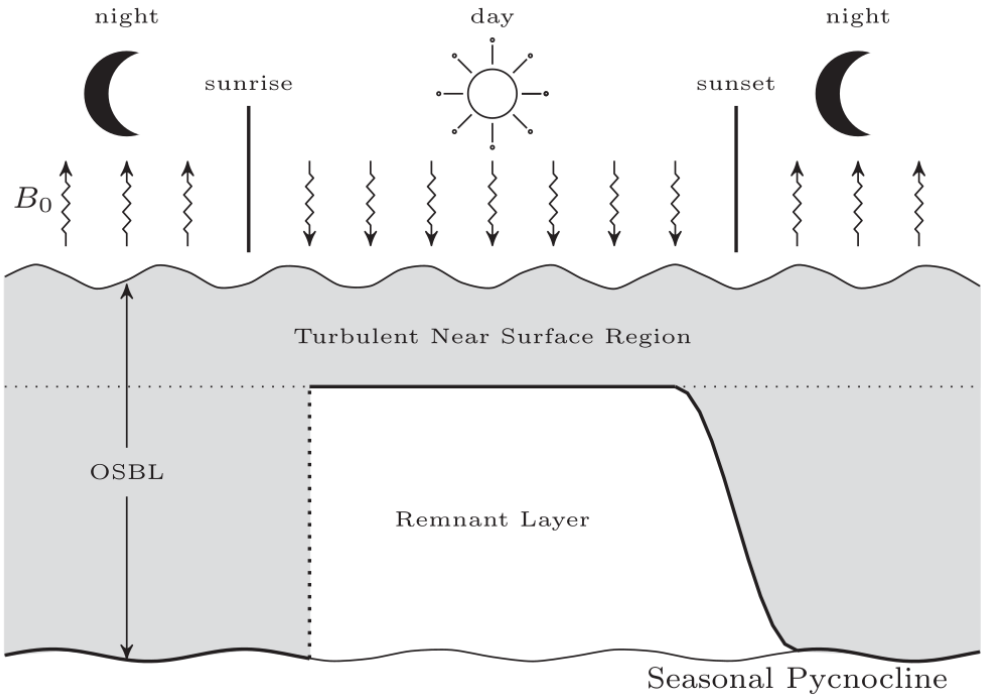

Figure 6.2: The diurnal cycle of the upper ocean during fair weather, i.e. sunny days with calm winds. Solar heating decouples a thin surface layer from the water below, thus creating a remnant layer that is isolated from the atmospheric forcing. Daytime winds create near surface shear flows that erode the thermocline between the surface and the remnant layer. At night the ocean loses heat, and overturning resets the ocean surface boundary layer structure (from Sutherland et al., 2016).

The diurnal cycle can be studied using simple and conceptual "Price-Weller-Pinkel type" models (Price et al., 1986). Such models include budgets for the momentum, heat, and freshwater content in the ocean surface boundary layer above the seasonal pycnocline, and use turbulence mixing schemes based on bulk and gradient Richardson numbers. An idealized depiction of the diurnal cycle is shown in Fig. 6.2. At night the net heat flux is negative, which leads to overturning. In the morning the boundary layer is therefore well mixed. As the sun starts to heat the ocean, the temperature stratification and associated turbulence suppression decouples the upper few meters from the rest of the boundary layer, leaving behind a remnant layer that becomes isolated from the atmospheric forcing. The wind ramps up during the day and shear-flow turbulence starts to erode the thermocline at the base of the surface layer, leading to a mixing of heat into the remnant layer below. Finally, when the sun sets and the net heat flux becomes negative, the heat loss will eventually lead to overturning and a new cycle can start next morning.

The decoupling of the surface layer means that the entire momentum flux from the atmosphere goes into a much thinner layer than in the absence of strong solar forcing, and thus the velocities in this layer become much larger. These strong currents are referred to as the *diurnal jet*. The more intense the shortwave forcing is, the shallower the surface layer will be, which leads to increasingly stronger jet. On the other hand, a strong jet in a very thin layer obviously leads to large rates of shear-flow turbulence production so that the near surface thermocline erodes more quickly. The overall amplitudes of the diurnal cycle are therefore variable and depend on the magnitudes of the momentum flux τ, the net heat flux Q and the vertical gradient in the net heat flux due to the absorption of shortwave radiation $\partial Q/\partial z$ (see also Fig. 6.3).

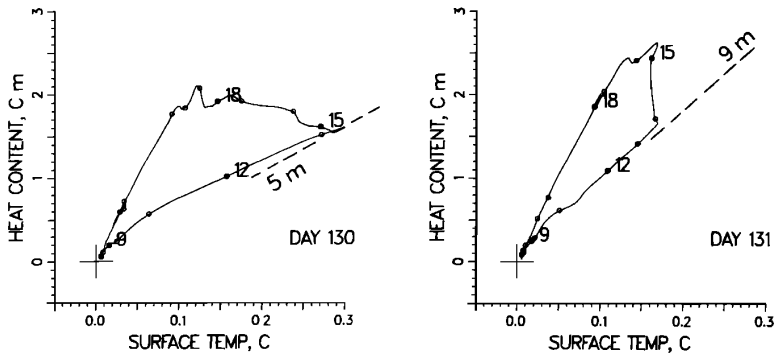

Figure 6.3: Hysteresis curves (solid lines) illustrating the diurnal cycle. Data from the West Pacific at about 30 degrees north. In the morning (indicated by the "+" sign) both the boundary layer heat content anomaly and the difference between the surface and bulk temperatures are close to zero. Absorption of shortwave energy increases both the heat content and the surface-bulk temperature difference. In the afternoon the shortwave flux becomes small and wind-forced turbulent entrainment of heat becomes dominant, which reduces the temperature difference but not the heat content. Finally, during the night the heat flux becomes negative and the upper ocean heat content is reduced (from Price et al., 1986, panels 3 and 4 from their Fig. 2).

6.4 Inertial oscillations with waves

6.4.1 The Coriolis-Stokes force

In earlier sections we discussed the mean momentum in the surface waves, and how this momentum is represented by the Stokes drift. As we saw in Sec. 6.2, transient changes in atmospheric forcing generate time dependent inertial currents, and these currents are influenced by the wave-induced drift as shown below. First of all, we will derive the Coriolis-Stokes force (Ursell, 1950; Hasselmann, 1970), which is an addition to the Coriolis force that is added to the Eulerian momentum equations whenever surface waves are present. The Coriolis-Stokes force can be derived in several ways, e.g. using a direct Lagrangian approach (Weber, 1983), quasi-Lagrangian coordinates (Broström et al., 2008) or by evaluation of the wave Reynolds stresses as in Hasselmann (1970).

For the derivation we will ignore horizontal gradients in the mean quantities. We will also neglect laminar stresses, assuming that the Reynolds stresses dominate. Expanding $\boldsymbol{u} = \bar{\boldsymbol{u}} + \tilde{\boldsymbol{u}} + \boldsymbol{u}'$, and after averaging over the turbulence and wave scales, the mean momentum equation becomes:

$$\frac{\partial \bar{\boldsymbol{u}}}{\partial t} + \boldsymbol{f} \times \bar{\boldsymbol{u}} = -\frac{\partial}{\partial z}\{\tilde{w}\tilde{\boldsymbol{u}}_{\mathrm{h}}\} - \frac{\partial}{\partial z}\langle w'\boldsymbol{u}'_{\mathrm{h}}\rangle. \tag{6.4.1}$$

The turbulent Reynolds stresses carry the momentum fluxes from the atmosphere and waves into the mean flow, which means that

$$-\frac{\partial}{\partial z}\langle w'\boldsymbol{u}'_{\mathrm{h}}\rangle = \rho^{-1}\frac{\partial \boldsymbol{\tau}}{\partial z}. \tag{6.4.2}$$

Now we use the linearized equation for the wave motion, *retaining the Coriolis term*. Noting that the pressure gradient force is orthogonal to w:

$$-\frac{\partial}{\partial z}\{\tilde{w}\tilde{\boldsymbol{u}}_{\mathrm{h}}\} = -\frac{\partial}{\partial z}\{\tilde{w}\int(\rho^{-1}\nabla_{\mathrm{h}}\tilde{p} - \boldsymbol{f}\times\tilde{\boldsymbol{u}})\,\mathrm{d}t\} = -\boldsymbol{f}\times\bar{\boldsymbol{u}}_{\mathrm{S}}. \tag{6.4.3}$$

The right-hand side here is the Coriolis-Stokes force (per unit density). It should properly be part of the forcing in any Eulerian general ocean circulation model. In practice the implementation of the Coriolis-Stokes force is not so straightforward, despite the fact that all the information needed is readily available. The reason is that the Coriolis-Stokes force, just like the usual Coriolis force, acts like a body force, and hence it needs to be distributed over the vertical layers in the

ocean model. To do this properly we need to integrate the two-dimensional wave spectrum over *all* wave directions and frequencies for *every* vertical level, at *every* horizontal grid point, and at *every* output time step for which the forcing is needed, see (3.4.8). Such computations quickly become too costly for operational forecasting systems but fortunately good approximations to the Stokes drift profile exist that are based on the much more readily available spectral moments (Breivik et al., 2016; Breivik and Christensen, 2020).

We now return to the integrated momentum equations (6.2.1) and (6.2.2). For simplicity, we ignore horizontal gradients, the Rayleigh friction terms and any currents in the deep ocean. We define the transports such that

$$\bar{\boldsymbol{U}} = \int_{-\infty}^{0} \bar{\boldsymbol{u}}\,\mathrm{d}z.$$

Using (6.4.1), (6.4.2) and (6.4.3):

$$\frac{\partial \bar{\boldsymbol{U}}}{\partial t} + \boldsymbol{f} \times (\bar{\boldsymbol{U}} + \bar{\boldsymbol{U}}_{\mathrm{S}}) = \frac{\boldsymbol{\tau}_{\mathrm{o}}}{\rho}, \tag{6.4.4}$$

where $\boldsymbol{\tau}_{\mathrm{o}}$ is the effective stress acting on the ocean as defined in (4.2.4). Recall that the mean wave momentum is the Stokes transport multiplied by the density:

$$\boldsymbol{M}_{\mathrm{w}} = \rho \bar{\boldsymbol{U}}_{\mathrm{S}}. \tag{6.4.5}$$

Going back to (4.2.4), again ignoring horizontal gradients, we see that we can write the effective stress on the ocean as

$$\boldsymbol{\tau}_{\mathrm{o}} = \boldsymbol{\tau}_{\mathrm{a}} - \rho \frac{\partial \bar{\boldsymbol{U}}_{\mathrm{S}}}{\partial t}. \tag{6.4.6}$$

We now define the Lagrangian transport

$$\bar{\boldsymbol{U}}_{\mathrm{L}} = \int_{-\infty}^{0} (\bar{\boldsymbol{u}} + \bar{\boldsymbol{u}}_{\mathrm{S}})\,\mathrm{d}z.$$

Then from (6.4.4) and (6.4.6), we finally find that

$$\frac{\partial \bar{\boldsymbol{U}}_{\mathrm{L}}}{\partial t} + \boldsymbol{f} \times \bar{\boldsymbol{U}}_{\mathrm{L}} = \frac{\boldsymbol{\tau}_{\mathrm{a}}}{\rho}. \tag{6.4.7}$$

In the absence of any atmospheric forcing of either the mean flow *or* the waves, this equation simply describe inertial oscillations of the total upper ocean transport $\bar{\boldsymbol{U}}_{\mathrm{L}}$, that is, inertial oscillations in a *Lagrangian* sense. The Coriolis-Stokes force will typically contribute to some extra veering of the surface currents (Polton et al., 2005), and since it acts at right angles to the total momentum, it does not directly contribute to the total mean kinetic energy (Weber et al., 2015).

6.4.2 Near inertial waves

Near inertial waves (NIW) are waves that are influenced by rotation (Sec. 8 of Gill, 1982, is an excellent reference). One classical example is that of Poincaré waves, which are plane surface waves with a dispersion relation

$$\omega^2 = f^2 + \omega_0^2, \tag{6.4.8}$$

where $\omega_0 = \kappa\sqrt{gH}$ is the frequency of shallow water gravity waves in the absence of rotation, with $\kappa = \sqrt{k^2 + l^2}$ being the horizontal wave number and H the local water depth. It is clear that $\omega > \omega_0$. One property of Poincaré waves is that the plane of motion changes from being entirely vertical to entirely horizontal in the limits $\omega \to \omega_0$ and $\omega \to f$, respectively. In the former case we simply have a shallow water gravity wave, while in the latter case we have pure inertial motion, or inertial oscillations, so that any passively drifting object will describe anticyclonic circular trajectories. In this limit of an infinitely long wave, the group velocity goes to zero (the energy equipartition principle of Sec. 2.2 does not apply to Poincaré waves).

With the exception of the simplified linear Rayleigh friction model of Sec. 6.2, we have not discussed in what ways the upper ocean may lose energy to the deeper layers. Internal gravity waves can propagate from the base of the mixed layer into the ocean interior, and such waves can obviously also be influenced by rotation. The generation of these internal gravity waves will typically be due to time-varying changes in the mixed layer depth, for example associated with the passage of a low pressure system. For a single Fourier component, the dispersion relation of such internal waves may be written (Gill, 1982):

$$\omega^2 = f^2 + N^2\alpha^2. \tag{6.4.9}$$

where $\alpha = \kappa/m$ is the aspect ratio and m is the vertical wave number. N is the buoyancy frequency as before. The dispersion relations (6.4.8) and (6.4.9) are clearly analogous. If the horizontal component of the wave length is much larger than the vertical (as is typically the case), we have $\alpha \ll 1$, and hence ω will be close to f. At the same time, the vertical component of the group velocity c_{gz} is approximately

$$c_{gz} = -\frac{N^2\alpha^2}{mf},$$

so that the vertical transport of energy strongly depends on the aspect ratio and the vertical wave number, with short vertical wave lengths implying slow vertical transport (see e.g. Alford et al., 2016).

We will not go into details here, but will note that the NIWs might take the form of (i) higher mode waves that propagate downward, and are associated with strong shear and elevated turbulence levels, and (ii) low mode (mode-1) oscillations that propagate equatorward due to the beta-effect. The presence of coastlines makes the problem considerably more complicated, and additional coastally trapped modes may be generated (see e.g. Kelly, 2019).

6.5 Oceanic drift of buoyant materials

6.5.1 Vertical dynamical balance

Bouyant materials include for example plankton (e.g. fish eggs), plastics and oil droplets. Such materials have finite size and we will in the following refer to them as particles. In this way we can generalize and describe the dynamics of such materials that have the same physical characteristics on short time scales through the vertical distribution, or concentration $C(x, y, z, t)$ given in "particles per liter". For small particles we usually neglect inertia. Any particle situated at a given depth z is then advected horizontally by the Lagrangian velocity

$$\bar{\boldsymbol{u}}_{\mathrm{L}}(z) = \bar{\boldsymbol{u}}(z) + \bar{\boldsymbol{u}}_{\mathrm{S}}(z). \tag{6.5.1}$$

In the absence of any currents each particle will rise through the water column with a terminal velocity w_{t}. This velocity is a function of the buoyancy of the particle and the Reynolds number $\mathrm{Re} = w_{\mathrm{t}} d/\nu$, where d is the diameter of the particle and ν is the kinematic viscosity. Depending on the buoyancy and the particle size, the upward motion may be laminar or (partially) turbulent. For example, Sundby (1983) assumes laminar flow for $\mathrm{Re} < 0.5$. The terminal velocity is then given by the Stokes equation:

$$w_{\mathrm{t}} = \frac{1}{18} \frac{g d^2 \Delta\rho}{\nu}, \tag{6.5.2}$$

where $\Delta\rho$ is the density difference. For $\mathrm{Re} > 0.5$ it is assumed that the motion is not fully turbulent, but that there is an intermediate regime in which the terminal velocity is

$$w_t = K_{\mathrm{I}} d_0 \left(\frac{\Delta\rho^2}{\nu} \right)^3. \tag{6.5.3}$$

Here the K_{I} is a constant and the $d_0 = d - \zeta D$, where d is the true diameter and D is the largest diameter for which (6.5.2) applies. Finally we have the constant $\zeta =$

0.4, which means that the effective diameter d_0 is reduced by at most 40% from the true diameter (obviously we need to require that $d > D$). Other formulations for the terminal velocity can of course be used and tested.

Assuming a steady state, the requirement that the mass is conserved leads to an advection-diffusion equation for the particle concentration C:

$$\frac{\partial}{\partial z}(w_{\mathrm{t}} C) = \frac{\partial}{\partial z}\left(K_{\mathrm{t}} \frac{\partial C}{\partial z}\right), \tag{6.5.4}$$

where $K_{\mathrm{t}}(z)$ is the depth dependent eddy diffusivity. Since $C \to 0$ and $\partial C/\partial z \to 0$ as $z \to -\infty$ (buoyant particles!) we can simply integrate (6.5.4) and we obtain

$$\frac{\partial}{\partial z}(\ln C) = \frac{w_{\mathrm{t}}}{K_{\mathrm{t}}}. \tag{6.5.5}$$

We have also used

$$\frac{1}{C}\frac{\partial C}{\partial z} = \frac{\partial}{\partial z}(\ln C).$$

Defining the surface concentration $C_0 = C(z = 0)$, we can integrate this equation and finally arrive at

$$C(z) = C_0 \exp\left(-\int_z^0 (w_{\mathrm{t}}/K_{\mathrm{t}})\,\mathrm{d}z'\right). \tag{6.5.6}$$

The simplest case is that of a constant eddy diffusivity and constant rise velocity (Sundby, 1983), then $C(z) = C_0 \exp[(w_{\mathrm{t}}/K_{\mathrm{t}})z]$. Large K_{t} and small w_{t} means that the material is distributed over a large depth (and *vice versa*) that scales as $D \propto K_{\mathrm{t}}/w_t$. Using the particle concentration C, we may introduce an effective transport velocity $\boldsymbol{u}_{\mathrm{C}}$ and a characteristic concentration depth scale D_{C} (Drivdal et al., 2015):

$$\boldsymbol{u}_{\mathrm{C}} = \frac{\int_{-\infty}^0 \bar{\boldsymbol{u}}_{\mathrm{L}} C\,\mathrm{d}z}{\int_{-\infty}^0 C\,\mathrm{d}z}, \tag{6.5.7}$$

$$D_{\mathrm{C}} = \frac{\int_{-\infty}^0 C\,\mathrm{d}z}{C_0}. \tag{6.5.8}$$

The concentration depth scale can be compared with other depth scales, for example the Ekman depth δ_{E}, for a qualitative assessment of the horizontal dispersion.

6.5.2 Some applications

See https://opendrift.github.io/.

Appendix A

Governing equations

A.1 The material derivative

The total (material) derivative is the temporal derivative (using the chain rule) following a material particle with velocity $\boldsymbol{u}$,

$$\frac{\mathrm{D}\gamma}{\mathrm{D}t} \equiv \frac{\partial \gamma}{\partial t} + \boldsymbol{u} \cdot \boldsymbol{\nabla}\gamma. \tag{A.1.1}$$

Here, γ can be any conserved scalar or vectorial quantity.

A.2 The mass conservation equation

The mass conservation equation

$$\frac{\partial \rho}{\partial t} + \boldsymbol{\nabla} \cdot (\rho \boldsymbol{u}) = 0 \tag{A.2.1}$$

can be considered an identity (Kundu, 1990). By rewriting it in terms of the material derivative,

$$\frac{\mathrm{D}\rho}{\mathrm{D}t} + \rho \boldsymbol{\nabla} \cdot \boldsymbol{u} = 0 \tag{A.2.2}$$

we see that if the fluid is incompressible, i.e., $D\rho/Dt = 0$, we get the continuity equation,

$$\boldsymbol{\nabla} \cdot \boldsymbol{u} = 0. \tag{A.2.3}$$

The mass conservation equation (A.2.1) simply expresses that a local change in density is a result of divergence/convergence in the advective transport. The equation (A.2.1) is given in so-called *conservative* or *flux* form, and is well suited for implementation in numerical solvers. The mass conservation equation in (A.2.3) is given in so-called *standard* form.

A.3 The momentum equation

The Navier-Stokes equation (Kundu, 1990), or momentum equation for a viscous fluid, is

$$\frac{\mathrm{D}\boldsymbol{u}}{\mathrm{D}t} = -\frac{1}{\rho}\boldsymbol{\nabla} p - g\hat{\boldsymbol{z}} + \boldsymbol{\nabla}\cdot(\boldsymbol{\tau}/\rho), \tag{A.3.1}$$

where p is the pressure, $\boldsymbol{\tau}$ the deviatoric (ie, the stress after the hydrostatic pressure is removed) stress tensor and $\hat{\boldsymbol{z}}$ the vertical unit vector (positive upwards). Eq (A.2.1) can be used to recast the momentum equation (A.3.1) in flux form,

$$\frac{\partial}{\partial t}(\rho\boldsymbol{u}) + \boldsymbol{\nabla}\cdot(\rho\boldsymbol{u}\boldsymbol{u}) = -\boldsymbol{\nabla} p - \rho g\hat{\boldsymbol{z}} + \boldsymbol{\nabla}\cdot\boldsymbol{\tau}. \tag{A.3.2}$$

This can also be written (Kundu 1990, p 85) in tensor form as

$$\frac{\partial \rho u_i}{\partial t} + \frac{\partial}{\partial x_j}(\rho u_i u_j) = -\frac{\partial p}{x_j} - \rho g\delta_{i3} + \frac{\partial \tau_{ij}}{\partial x_j}. \tag{A.3.3}$$

The same technique is used to rewrite scalar conservation equations for salinity and temperature.

A.4 The Coriolis effect

The fictitious Coriolis force must be included in a rotating (accelerated) frame of reference,

$$\frac{\mathrm{D}\boldsymbol{u}}{\mathrm{D}t} + 2\boldsymbol{\Omega}\times\boldsymbol{u} = -\frac{1}{\rho}\boldsymbol{\nabla} p - g\hat{\boldsymbol{z}} + \boldsymbol{\nabla}\cdot\boldsymbol{\tau}. \tag{A.4.1}$$

A simplified set of equations appears when we consider the f-plane approximation, where only the rotation perpendicular to the local plane on latitude ϕ is considered, $f = 2\Omega\sin\phi$,

$$\frac{\mathrm{D}\boldsymbol{u}}{\mathrm{D}t} + f\hat{\boldsymbol{z}}\times\boldsymbol{u} = -\frac{1}{\rho}\boldsymbol{\nabla} p - g\hat{\boldsymbol{z}} + \boldsymbol{\nabla}\cdot(\boldsymbol{\tau}/\rho). \tag{A.4.2}$$

A.5 Boussinesq approximation

The Boussinesq approximation states that density differences are negligible compared with the gravitational acceleration and hence only need be accounted for in the gravity term where it is multiplied by g (Kundu 1990, p 112). According to Pond and Pickard (1983), p 61,

> Boussinesq said that, if the density variations are fairly small, to a first approximation we can neglect their effect on the *mass* (ie, inertia) of the fluid but we must retain their effect on the *weight*. That is, we must included the buoyancy effects but can neglect the variations in horizontal accelerations for a given force due to the mass variations with density (which are at most 3% if we use an average over the whole ocean for ρ or α). Thus in the horizontal momentum equations (x- and y-directions) we can use an average density over the region being considered but in the z-equation, which reduces to the hydrostatic equation, we must use the actual in situ values when calculating the pressure field.

A.6 The turbulence kinetic energy equation

The turbulence kinetic energy equation is derived from the momentum equation (A.3.1) by taking the dot product with the velocity and performing Reynolds averaging. It can be written as [(Stull, 1988), p 152]

$$\frac{\mathrm{D}e}{\mathrm{D}t} = \frac{g}{\rho_\mathrm{w}}\overline{u_3'\rho'} - \overline{u_i'u_j'}\frac{\partial \overline{u}_i}{\partial x_j} - \overline{u_i'u_j'}\frac{\partial v_i}{\partial x_j} - \frac{\partial}{\partial x_j}(\overline{u_j'e}) - \frac{1}{\rho_\mathrm{w}}\frac{\partial}{\partial x_i}(\overline{u_i'p'}) - \epsilon. \quad \text{(A.6.1)}$$

Here, $e \equiv q^2/2 = \overline{u_i'u_i'}/2$ is the TKE per unit mass (with q the turbulent velocity) and ϵ is the dissipation [see e.g. Stull (1988) p 152].

By making the gradient transport closure approximation (Stull, 1988), ignoring advective terms and horizontal gradients, and rewriting in vectorial form we arrive at

$$\frac{\partial e}{\partial t} = -\nu_\mathrm{h}N^2 + \nu_\mathrm{m}S^2 + \nu_\mathrm{m}\boldsymbol{S}\cdot\frac{\partial \boldsymbol{u}_\mathrm{s}}{\partial z} - \frac{\partial}{\partial z}(\overline{w'e}) - \frac{1}{\rho_\mathrm{w}}\frac{\partial}{\partial z}(\overline{w'p'}) - \epsilon. \quad \text{(A.6.2)}$$

Here we have reverted to using z for the vertical axis and w for vertical velocities. We recognize in Eqs (A.6.1)–(A.6.2) the familiar terms of the TKE equation [see

Stull 1988, Eq (5.1a)], namely shear production, $S^2 = (\partial\overline{\boldsymbol{u}}/\partial z)^2$, and buoyancy production through the Brunt-Vaisälä frequency, $N^2 = -(g/\rho)\mathrm{d}\rho/\mathrm{d}z$ ($\nu_{\mathrm{m,h}}$ are turbulent viscosity and diffusion coefficients, respectively) as well as the divergences of the pressure correlation term $\overline{w'p'}$ and turbulent transport $\overline{w'e}$. We have also here included the shear of the Stokes drift, which is not usually included.

Bibliography

Alford, M.H., MacKinnon, J.A., Simmons, H.L., Nash, J.D., 2016. Near-Inertial Internal Gravity Waves in the Ocean. Annual Review of Marine Science 8, 95–123.

Breivik, O.y., Bidlot, J.R., Janssen, P.A.E.M., 2016. A Stokes drift approximation based on the Phillips spectrum. Ocean Modelling 100, 49–56.

Breivik, Ã., Christensen, K.H., 2020. A Combined Stokes Drift Profile under Swell and Wind Sea. J. Phys. Oceanogr. 50, 2819–2833.

Broström, G., Christensen, K.H., Drivdal, M., Weber, J.E.H., 2014. Note on Coriolis-Stokes force and energy. Ocean Dyn. 64, 1039–1045.

Broström, G., Christensen, K.H.k., Weber, J.E.H., 2008. A Quasi-Eulerian, Quasi-Lagrangian View of Surface-Wave-Induced Flow in the Ocean. Journal of Physical Oceanography 38, 1122–1130.

Buckingham, E., 1914. On Physically Similar Systems; Illustrations of the Use of Dimensional Equations. Physical Review 4, 345–376. doi:10.1103/PhysRev.4.345.

Canuto, V.M., Howard, A., Cheng, Y., Dubovikov, M.S., 2001. Ocean Turbulence. Part I: One-Point Closure Model Momentum and Heat Vertical Diffusivities. J. Phys. Oceanogr. 31, 14.

Craig, P.D., Banner, M.L., 1994. Modeling Wave-Enhanced Turbulence in the Ocean Surface Layer. J. Phys. Oceanogr. 24, 2546–2559.

Drivdal, M., Broström, G., Christensen, K.H., 2015. Wave-induced mixing and transport of buoyant particles: application to the Statfjord A oil spill. Ocean Sci. 10, 977–991.

Ekman, V.W., 1905. On the influence of the earth's rotation on ocean-currents. Ark. Mat. Astron. Fys. 2, 1–52.

Gemmrich, J., Mudge, T., Polonichko, V., 1994. On the energy input from wind to surface waves. J. Phys. Oceanogr. 24, 2413–2417.

Gill, A.E., 1982. Atmosphere-ocean dynamics. International geophysics series, Academic Press, New York.

Gradshteyn, I., Ryzhik, I., 2007. Table of Integrals, Series, and Products, 7th edition. Edited by A. Jeffrey and D. Zwillinger, Academic Press, London.

Hasselmann, K., 1970. Wave driven inertial oscillations. Geophys. Fluid Dyn. 1.

Holthuijsen, L., 2007. Waves in Oceanic and Coastal Waters. Cambridge University Press.

Janssen, P.A.E.M., 2012. Ocean wave effects on the daily cycle in SST. J. Geophys. Res. 117, 24 pages.

Kato, H., Phillips, O.M., 1969. On the penetration of a turbulent layer into stratified fluid. J. Fluid Mech. 37, 643–655.

Kelly, S.M., 2019. Coastally Generated Near-Inertial Waves. Journal of Physical Oceanography 49, 2979–2995.

Kundu, P.J., 1990. Fluid Mechanics. Academic Press, London.

Large, W.G., McWilliams, J.C., Doney, S.C., 1994. Oceanic vertical mixing: A review and a model with a nonlocal boundary layer parameterization. Rev. Geophys. 32, 363–403.

Longuet-Higgins, M.S., 1953. Mass Transport in Water Waves. Phil. Trans. Roy. Soc. A 245, 535–581.

Longuet-Higgins, M.S., 1969. A nonlinear mechanism for the generation of sea waves. Proc. Roy. Soc. London A , 371–389.

Madsen, O.S., 1977. A realistic model of the wind-induced Ekman boundary layer. J. Phys. Oceanogr. 7, 248–255.

McWilliams, J., Sullivan, P.P., 2000. Vertical mixing by Langmuir circulations. Spill Science & Technology Bulletin 6, 225–237.

Ortiz-Suslow, D.G., Wang, Q., Kalogiros, J., Yamaguchi, R., 2020. A method for identifying Kolmogorov's inertial subrange in the velocity variance spectrum. J. Atmos. Ocean. Technol. 37, 85–102.

Phillips, O.M., 1977. The Dynamics of the Upper Ocean. 2 ed., Cambridge University Press, Cambridge.

Pollard, R.T., Millard, R., 1970. Comparison between observed and simulated wind-generated inertial oscillations. Deep-Sea Res I 17, 813–821.

Polton, J.A., Lewis, D.M., Belcher, S.E., 2005. The role of wave-induced Coriolis-Stokes forcing on the wind-driven mixed layer. Journal of Physical Oceanography 35, 444–457.

Pond, S., Pickard, G., 1983. Introductory Dynamical Oceanography, 2nd edition. Pergamon.

Price, J.F., Weller, R.A., Pinkel, R., 1986. Diurnal cycling: Observations and models of the upper ocean response to diurnal heating, cooling, and wind mixing. J. Geophys. Res. 91, 8411.

Röhrs, J., Christensen, K.H., 2015. Drift in the uppermost part of the ocean. Geophysical Research Letters , 8 pp.

Sprintall, J., Cronin, M., 2001. Upper Ocean Vertical Structure, in: Encyclopedia of Ocean Sciences. Elsevier, pp. 3120–3128.

Stokes, G.G., 1847. On the theory of oscillatory waves. Trans. Cambridge Philos. Soc. 8, 441–473.

Stull, R.B., 1988. An introduction to boundary layer meteorology. Kluwer, New York.

Sundby, S., 1983. A one-dimensional model for the vertical distribution of pelagic fish eggs in the mixed layer. Deep Sea Res. 30, 645–661.

Sutherland, G., Marié, L., Reverdin, G., Christensen, K.H., Broström, G., Ward, B., 2016. Enhanced Turbulence Associated with the Diurnal Jet in the Ocean Surface Boundary Layer. J. Phys. Oceanogr. 46, 3051–3067.

Sutherland, G., Ward, B., Christensen, K.H., 2013. Wave-turbulence scaling in the ocean mixed layer. Ocean Sci. 9, 597–608.

Turner, J.S., Kraus, E.B., 1967. A one-dimensional model of the seasonal thermocline I. *A laboratory experiment and its interpretation*. Tellus 19, 88–97.

Umlauf, L., Burchard, H., 2003. A generic length-scale equation for geophysical turbulence models. J. Mar. Res. 61, 235–265.

Ursell, F., 1950. On the theoretical form of ocean swell on a rotating earth. Geophys. J. International 6, 1–8.

Warner, J.C., Sherwood, C.R., Arango, H.G., Signell, R.P., 2005. Performance of four turbulence closure models implemented using a generic length scale method. Ocean Model. 8, 81–113.

Weber, J.E., 1983. Attenuated wave-induced drift in a viscous rotating ocean. J. Fluid Mech. 137, 115–129.

Weber, J.E., 2001. Virtual wave stress and mean drift in spatially damped surface waves. J. Geophys. Res. 106, 11653–11657.

Weber, J.E.H., 2019. Lagrangian studies of wave-induced flows in a viscous ocean. Deep Sea Res. 160, 68–81.

Weber, J.E.H., Broström, G., Saetra, Ø., 2006. Eulerian versus Lagrangian approaches to the wave-induced transport in the upper ocean. J. Phys. Oceanogr. 36, 2106–2118.

Weber, J.E.H., Drivdal, M., Christensen, K.H., Broström, G., 2015. Some aspects of the Coriolis-Stokes forcing in the oceanic momentum and energy budgets. Journal of Geophysical Research 120, 5589–5596.